Structure—Property Relationships for Exciton Transfer in Conjugated Polymers

Trisha L. Andrew, Timothy M. Swager

Massachusetts Institute of Technology, Department of Chemistry, 77 Massachusetts Avenue, Cambridge, Massachusetts 02139

Correspondence to: T. M. Swager (E-mail: tswager@mit.edu)

Received 25 January 2011; accepted 25 January 2011; published online
DOI: 10.1002/polb.22207

ABSTRACT: The ability of conjugated polymers to function as electronic materials is dependent on the efficient transport of excitons along the polymer chain. Generally, the photophysics of the chromophore monomer dictate the excited state behavior of the corresponding conjugated polymers. Different molecular structures are examined to study the role of excited state lifetimes and molecular conformations on energy transfer. The incorporation of rigid, three-dimensional scaffolds, such as iptycenes and cyclophanes, can encourage an oblique packing of the chromophore units of a conjugated polymer, thus allowing the formation of electronically-coupled aggregates that retain high quantum yields of emission. Rigid iptycene scaffolds also act as excellent structural directors that encourage complete solvation of PPEs in a liquid crystal (LC) solvent. LC-PPE mixtures display both an enhanced conformational alignment of polymer chains and extended effective conjugation lengths relative to isotropic solutions, which leads to enhanced energy transfer. Facile exciton migration in poly(*p*-phenylene ethynylene)s (PPEs) allows energy absorbed over large areas to be funneled into traps created by the binding of analytes, resulting in signal amplification in sensory devices. © 2011 Wiley Periodicals, Inc. J Polym Sci Part B: Polym Phys 49: 476–498, 2011

KEYWORDS: acridine orange (AO); conjugated polymers (CPs); fluorescent polymers; Langmuir–Blodgett assembly; liquid crystals (LC); poly(*p*-phenyl ethynylene)s (PPE)

INTRODUCTION Conjugated polymers (CPs) are useful materials that combine the optoelectronic properties of semiconductors with the mechanical properties and processing advantages of plastics. In general, CPs in their neutral state are wide band-gap semiconductors with direct band gaps.[1] Many CPs have an extremely large absorption cross-section ($\sigma \approx 10^{-15}$ cm^2) because the $\pi \rightarrow \pi^*$ transition is allowed and the quasi one-dimensional electronic wavefunctions have a high density of states at the band edge.[2] Additionally, a CP can exhibit strong luminescence depending on the system. The luminescence efficiency is primarily related to the delocalization and polarization of the electronic structure of the CP.[1]

A vast number of studies on oligomers confirm that the electronic states in a CP have limited delocalization, and the electronic structure of a given CP is often determined by 7–13 repeating units. This is particularly prevalent in systems containing aromatic rings since the aromatic character localizes the electronic wavefunctions. As a result of this localization, a CP's band gap is largely determined by its local electronic structure.[1]

The emission of CPs is dominated by energy migration to local minima in their band structures. For example, the emission from electroluminescent devices occurs from regions with greatest conjugation[3] and the emission from complex ladder polymers can be dominated by defect sites present in low concentration.[4] However, a fundamental understanding of the relative mechanisms of energy migration in these systems remains elusive. This inherent difficulty is a result of the fact that CPs have disordered dynamic conformations that produce variable electronic delocalization, both within a given polymer and between neighboring polymer chains.[5] To improve this situation, it is necessary to design polymers with specific structures and properties intended to test proposed mechanisms of energy migration.

In this review, we look at the photophysical properties of an exciton transport in a series of poly(*p*-phenyl ethynylene) s (PPEs, see Fig. 1). First, the use of energy migration in PPEs to create signal gain in chemical sensors is discussed. Next, we detail the importance of dimensionality and molecular design in directing excitations and the effect of excited-state lifetime modulation on energy migration in PPEs. The ability to extend electronic delocalization and induce well-defined CP conformations in liquid crystal (LC) solutions is also discussed. We restrict our analysis to primarily PPEs.

SIGNAL GAIN IN AMPLIFYING FLUORESCENT POLYMERS

Rigid rod CPs, such as PPEs (Fig. 1), may be thought of as "molecular wires" with well-defined lengths proportional to molecular weight. Therefore, PPEs can be used to

Trisha L. Andrew received her B.S. in Chemistry from the University of Washington in 2005 and her Ph.D. in organic chemistry in 2011, under the supervision of Professor Timothy M. Swager. She is currently a postdoctoral researcher in the laboratory of Professor Vladimir Bulovic at the Organic and Nanostructured Electronics Lab at MIT.

Timothy M. Swager is the John D. MacArthur Professor of Chemistry at the Massachusetts Institute of Technology. A native of Montana, he received a BS from Montana State University in 1983 and a Ph.D. from the California Institute of Technology in 1988. Swager s research interests are in design, synthesis, and study of organic-based electronic, sensory, and liquid crystalline materials.

interconnect, or wire in series, receptors to produce fluorescent chemosensory systems with sensitivity enhancements over single receptor analogs.[6] In a PPE with a receptor attached to every repeat unit, the degree of polymerization defines the number of receptor sites, *n*. If energy migration is rapid with respect to the fluorescence lifetime, then the excited state can sample every receptor in the polymer, thereby allowing the occupation of a single binding site to dramatically change the entire emission of the PPE. In the event that a receptor site is occupied by a quencher, the result is an enhanced deactivation of the excited state.[6] For isolated polymer chains in solution, the sensitivity may be enhanced by as much as *n* times over single-molecule receptors; however, larger effects may occur in the solid state wherein interpolymer energy transfer may also occur.

This concept is demonstrated by studying the fluorescence-quenching responses of model compounds **1**–**2** and their corresponding PPEs, **P1**–**2** (see Fig. 3). The operative interaction that leads to quenching of fluorescence in these systems is the formation of a pseudorotaxane between a *bis*(*p*-phenylene)-34-crown-10 (BPP) moiety and paraquat, PQ^{2+}, a well-known electron transfer quenching agent (see Fig. 2).[7]

Electron transfer fluorescence quenching by PQ^{2+} can occur by either dynamic (collisional) or static (associated complex) processes. The dependence of the fluorescence intensity on the quencher concentration follows the Stern–Volmer relationship, whose general form is shown in eq. (1)[8]:

$$F_0/F = (1 + K_D[Q])\exp(V[Q]) \quad (1)$$

In this equation, F_0 and F are the fluorescence intensities in the absence and presence of the quencher, respectively, K_D denotes the dynamic quenching constant, and V represents the static quenching constant. When $[Q]$ or V is very small, the contribution from static quenching can be approximated by a linear function of quencher concentration and Eq. (1) simplifies to

$$F_0/F = (1 + K_D[Q])(1 + K_S[Q]) \quad (2)$$

where K_S now denotes the static quenching constant. Furthermore, if either a static or dynamic process dominates the quenching response, eq. (2) can be further simplified to include only one linear term:

$$F_0/F = 1 + K_{SV}[Q] \quad (3)$$

where K_{SV} is either the dynamic (K_D) or static (K_S) quenching constant. When the fluorophore and the quencher form a simple one-to-one dark complex, K_{SV} is equivalent to the association constant, K_a. However, for systems with more complex species, the quenching profile may deviate from the linear function and the more general form of the Stern–Volmer relationship (i.e., Eq. (1)) must be used.[8]

In static quenching, diffusion rate of the quencher is not a factor and the fluorescence lifetime of the fluorophore, τ, is independent of $[Q]$. However, for purely dynamic quenching, the excited state is quenched by a collision with the quencher and thus the lifetime is truncated with added quencher.[8] As a result, monitoring the changes in the lifetime of the fluorophore with added quencher represents the

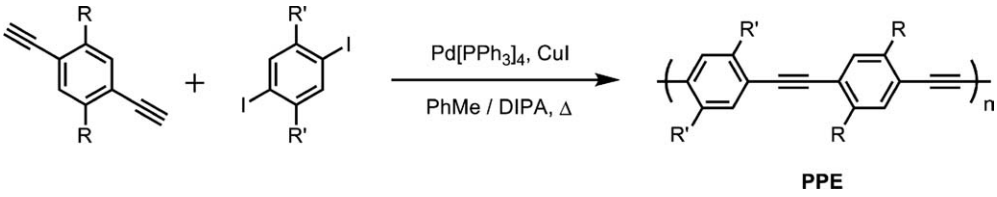

FIGURE 1 A general synthetic route to poly(*p*-phenylene ethynylene)s (PPEs).

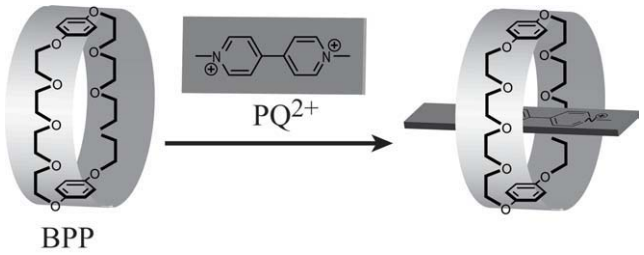

FIGURE 2 The formation of a pseudo-rotaxane between a *bis*(*p*-phenylene)-34-crown-10 (BPP) and paraquat (PQ^{2+}).

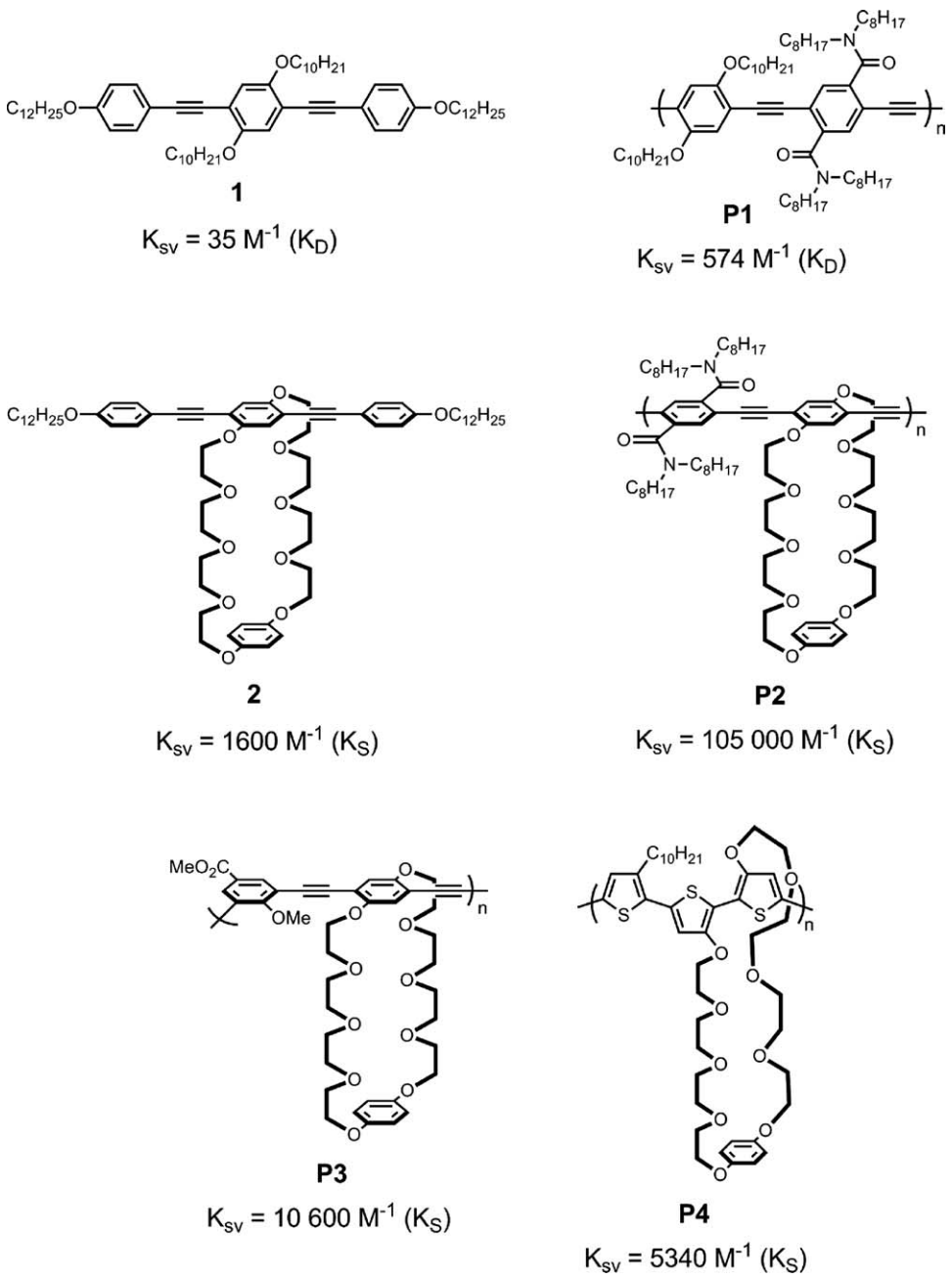

FIGURE 3 Structures of the model compounds and polymers used to investigate amplified fluorescence quenching and their associated quenching constants, K_{SV}.

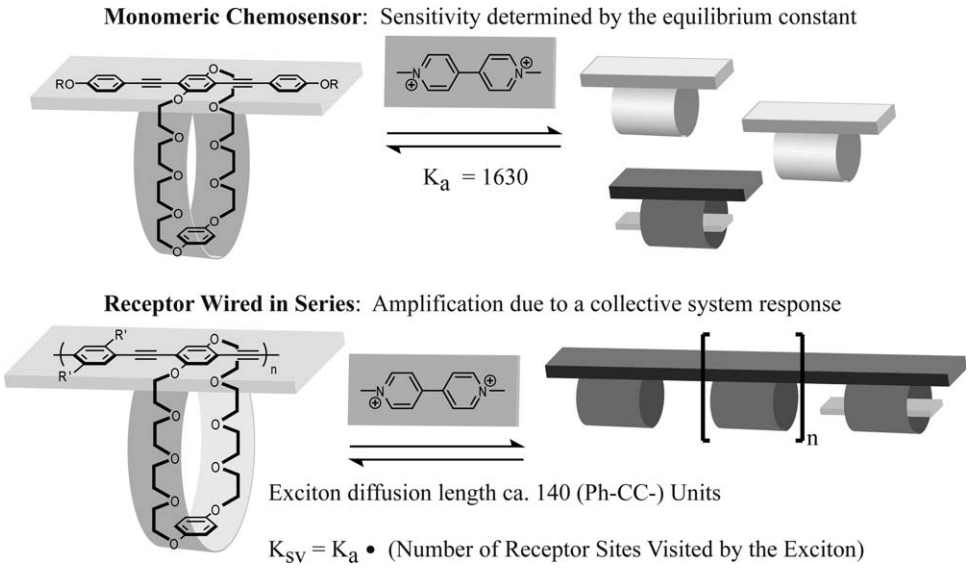

FIGURE 4 Schematic explaining the concept of signal amplification due to a collective system response.

conventional practice for determining the dynamic quenching constant independent of the static quenching process. The correlation of lifetime with quencher concentration can be expressed as

$$\tau_0/\tau = 1 + K_D[Q] \quad (4)$$

The structures of the model compounds and polymers used to investigate amplified fluorescence quenching are shown in Figure 3, along with their quenching constants with PQ^{2+}.[9] Comparing **1** and **P1**, a 16-fold enhancement in the dynamic quenching constant is observed upon transitioning from a small molecule to a CP (35 vs. 574 M^{-1}, respectively), even in a system lacking the BPP receptor. This enhancement results from the extended electronic structure of the polymer, which produces a mobile delocalized excited state and a larger effective size. It is important to note that this enhancement occurs in spite of the fact that the lifetime of **P1** (0.5 ns) is shorter than that of **1** (1.2 ns). When the BPP receptor is introduced, addition of PQ^{2+} results in the formation of a charge transfer (CT) complex with either an associated red-shifted absorption onset or the growth of a new CT band and static quenching dominates. A 66-fold increase in K_S value is observed for CP **P2** relative to small molecule **2**, in agreement with our model for signal amplification due to a collective system response (see Fig. 4).

The degree of enhancement resulting from energy migration is determined by the radiative lifetime and the mobility of the excitations in the polymer. Longer lifetimes and higher mobilities will produce longer average diffusion lengths. For isolated polymers in solution, if this diffusion length exceeds the length of the polymer, then an increase in molecular weight will produce greater enhancements. Accordingly, lower molecular weight analogs of **P2** display smaller values of K_S than higher molecular weight analogs: K_S = 105 000 M^{-1} for M_n 122 500 but K_S = 75 000 M^{-1} for M_n 31 100. However, it must be noted that the value of K_S remains largely unaffected after the molecular weight of the polymer exceeds ca. 65,000. This result reveals that the exciton was not able to visit the entire length of the higher molecular weight polymers because of its limited mobility and finite lifetime (there is always competitive relaxation to the ground state). Therefore, one can conclude that the exciton diffusion length in a PPE is approximately 140 (Ph-CC-) units.[9]

Additionally, the *para*-linked polymer **P2** is observed to be more effective at energy migration than both its *meta*-linked analog, **P3**, and a poly(thiophene) analog, **P4**. This difference exists in spite of the fact that the lifetime of **P3** (1.88 ns) is about a factor of 3 longer than that of **P2** (0.64 ns). The observation that excitations in **P3** have longer lifetimes indicates that energy migration is slower in this system relative to **P2**.

It can be argued that the greater tendency for energy migration in *para*-linked **P2** over *meta*-linked **P3** might be expected based on delocalization; however, greater delocalization is not a guarantee of superior performance. This fact is illustrated by polymer **P4**, which displays a K_S value of only 5340 M^{-1}. This result indicates that **P4** is less effective at energy migration than **P2**, even though poly(thiophene)s display much greater bandwidths (delocalization) relative to PPEs.

DIRECTING ENERGY TRANSFER WITHIN CPS: DIMENSIONALITY AND MOLECULAR DESIGN

Solutions vs Thin Films

As stated before, the emission of CPs is often dominated by energy migration to local minima in their band structures. For example, selective emission from states associated with anthracene end groups has been demonstrated in solutions of PPEs (see Fig. 5).[10] As is characteristic for most PPEs, **P5** displays a broad absorption band centered at 446 nm and a

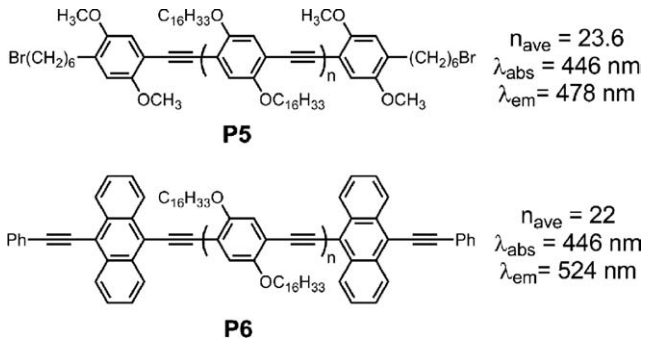

FIGURE 5 Structures of the PPEs used to demonstrate efficient energy transfer to low-energy anthracene end groups.

relatively sharp emission spectrum with vibronically resolved (0,0) and (0,1) bands centered at 478 and 510 nm, respectively. In the case of **P6**, however, where terminal anthracene units are present, the solution emission spectrum is dominated by a single band at 524 nm, which corresponds to emission from the anthracene end group. The fluorescence quantum yields of **P5** and **P6** are roughly comparable (0.35 and 0.28, respectively), the emission spectra of both polymers are insensitive to the excitation wavelength and their corrected excitation spectra match the absorption spectra, thus confirming that the 524 nm band of **P6** results from excitation of the bulk material and subsequent energy migration to the lower energy end groups. By comparison of the emission intensities of the 524 nm band and a residual 474 nm band (that corresponds to fluorescence from the PPE backbone) in the emission spectrum of **P6**, it was concluded that the energy transfer from the polymer backbone to the anthracene end-groups proceeded with >95% efficiency in solution.

Energy transfer in a related PPE, **P7**, (see Fig. 6) however, was found to be more sensitive to the physical state of the system. In solutions of **P7**, emission from both the polymer backbone and anthracene end-group can be observed in an approximately 2:1 ratio. On the other hand, thin films of **P7** *exclusively* display emission from the anthracene end groups at 492 nm. Therefore, transitioning from a 1D solution system to 3D thin films enables intra- and interpolymer energy transfer, which results in more extensive exciton migration to energy minima.

Although PPEs superficially appear to have rigid-rod structures, materials with higher degrees of polymerization exhibit coiled solution structures with persistence lengths of approximately 15 nm.[11] For isolated polymer chains in dilute solutions, the migration of excitations along the polymer backbone follows the random walk statistics of 1D diffusion. Therefore, given that the exciton diffusion length in PPEs is ca. 140 (Ph-CC-) units (see Signal Gain in Amplifying Fluorescent Polymers section), 1D exciton transport requires $(140)^2$ hops to travel 140 linear hops. Although this means that the exciton can theoretically sample approximately 20,000 phenylethynyl repeat units, 1D random walks do not

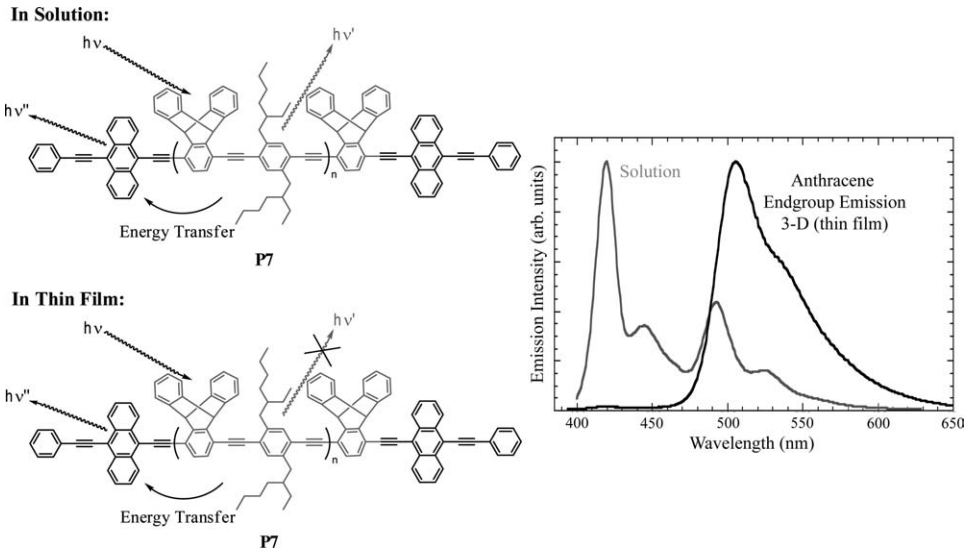

FIGURE 6 Structure and emission spectrum of an anthracene end-capped PPE that displays notably different behavior in isotropic solutions and thin films.

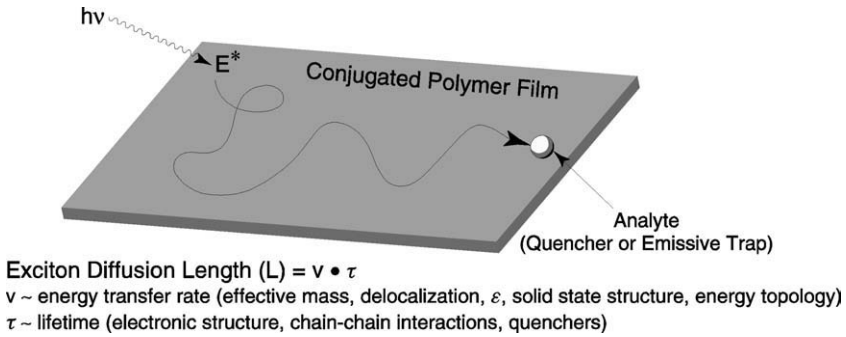

FIGURE 7 Factors that influence three-dimensional exciton migration in thin films of conjugated polymers.

provide the optimal pathway for energy migration (and thus signal amplification) because an excitation necessarily retraces portions of the polymer backbone multiple times. Hence, it is necessary to enable 2D and 3D random walks of the excitations. This increased dimensionality decreases the probability of an excitation retracing a given segment of the polymer and thereby produces a larger amplification in sensory schemes.

It is for this reason that thin films of CPs can serve as unparalled, highly sensitive chemosensors (exemplarily for 2,4,6-trinitrotoluene (TNT)[12]). In general, increases in the diffusion length of the exciton within the CP thin film will enhance the sensitivity of the chemosensor. As shown in Figure 7, the exciton diffusion length (L) is provided by the product of the energy transfer rate (v) and lifetime (τ) of the exciton. The energy transfer rate, v, is dependent in part, on the extent of delocalization in the polymer, the effective mass of the exciton, and the energy surface topology of the CP thin film. The lifetime of the exciton is largely defined by the photophysics of the polymer repeat unit and can be further influenced by the presence of interchain interactions and quenchers.

Within thin films, individual polymer chains electronically couple, thus encouraging interpolymer energy transfer. The efficiency of intermolecular energy migration depends on

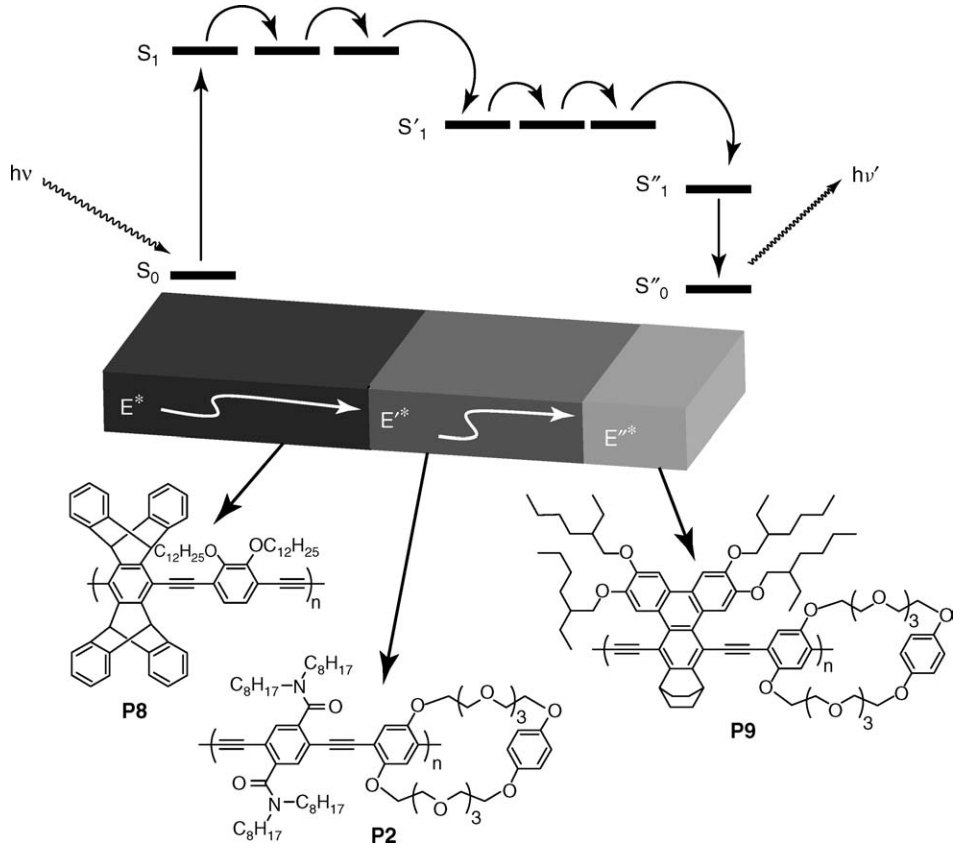

FIGURE 8 A striated multipolymer system that demonstrates vectorial energy transfer normal to the substrate. Adapted with permission from ref. 14. Copyright 2001 American Chemical Society.

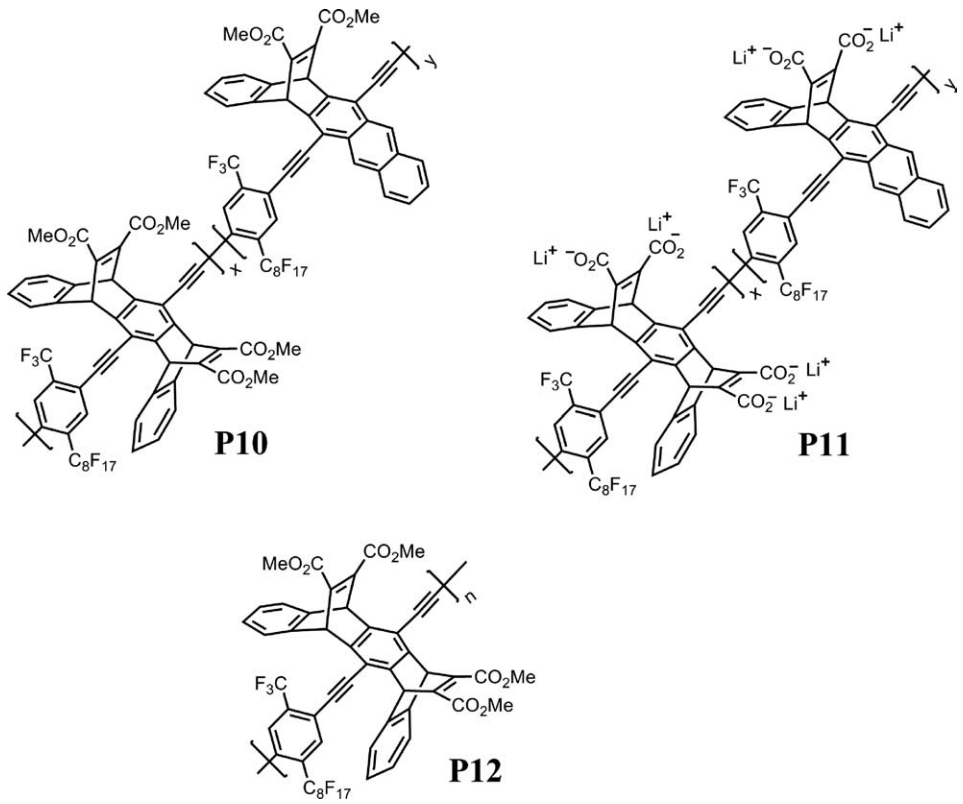

FIGURE 9 Structures of anthryl-incorporated PPEs and a corresponding PPE lacking low-energy trap sites.

facile dipolar Förster-type processes, which are optimal when the transition dipoles of the donor and acceptor groups are aligned. As a result, films of aligned polymers with extended chain conformations provide an ideal situation for energy migration. Such optimal polymer conformations are best achieved by forming monolayer or multilayer films of PPEs prepared by the Langmuir–Blodgett (LB) deposition technique.[13]

For example, a striated multipolymer system composed of three different PPEs with tailored absorption and emission maxima designed to have large spectral overlap between a donor emission and an acceptor absorption can be precisely fabricated using the LB technique (see Fig. 8).[14] In this system, spectral overlap encourages energy transfer from **P8** to **P2** and from **P2** to **P9**. Polymers **P2** and **P9** are also nonaggregating and amphiphilic, thus allowing manipulations at the air–water interface. The trilayer assembly was created by first spin-coating the shortest-wavelength polymer, **P8**, on a glass substrate. Next, 16 LB layers of **P2** were coated over this spin-cast film and finally a single monolayer of **P9** was coated, thus providing a composite film where the band gap decreases directionally from the substrate to the polymer–air interface. Excitation of the three-component film at 390 nm (λ_{max} of **P8**) resulted in an emission spectrum consisting of three peaks: two small peaks at 423 and 465 nm, which are attributed to emission from **P8** and **P2**, respectively, and a third, dominant peak at 512 nm that is a result of energy transfer from **P8** and **P2** to **P9** and subsequent emission from **P9**. The observation that most of the excitation energy is transferred from **P8** through 16 layers of **P2** to **P9** demonstrates that energy can be efficiently moved in the *z*-direction, thereby concentrating the energy at the film–air interface. Direct excitation of **P9** at 490 nm resulted in a peak at 512 nm of much lower fluorescence intensity than the peak resulting from excitation at 390 nm; the difference in fluorescence intensity is directly proportional to the difference in optical density at 390 nm versus 490 nm, again confirming the efficiency of energy transfer.

Aggregates

Continuing with the aforementioned practice of using anthracene moieties as low energy emissive traps, PPEs **P10** and **P11** (see Fig. 9) incorporating anthryl units were synthesized and investigated (polymer **P11** is simply a polyelectrolytic analog of **P10**)[15,16]. In contrast to polymers **P6** and **P7**, which contained anthracene moieties as end groups, polymers **P10** and **P11** are random copolymers containing small concentrations (1–9%) of an anthryl comonomer. However, the optical effects of incorporating anthryl moieties into the polymer backbone are largely similar to those observed with **P6** and **P7**: new, intense, long-wavelength emission bands that are sensitive to the dimensionality of the system are observed. For example, the effect of anthracene incorporation can best be appreciated upon comparing the emission spectra of **P10** with that of **P12**, which is an anthryl-free analog of **P10**. PPE **P12** displays the characteristic two-band emission spectrum of PPEs, with an emission maximum at 433 nm in solutions and in thin films. Solution emission spectra of **P10** exhibit these same two bands, but also display a

third, green emission band centered between 500 and 520 nm (depending on the percent of anthryl comonomer) that greatly increases in intensity in thin films of **P10**. Furthermore, **P10** has a long (1.5–1.9 ns) excited-state lifetime, as compared to **P12** (0.44 ns).

As discussed before, the green band emission from **P10** is much more pronounced when the polymer is in its film state than when it is dissolved in dilute solutions because of the enhanced exciton migration present in CP films (3D) relative to that present in dilute polymer solutions (1D). In dilute solutions only, *intra*chain exciton migration is possible because individual polymer chains are isolated from one another. However, in the film state, chains of **P10** are aggregated within close proximity to each other such that *inter*chain exciton migration becomes possible. If the low-energy exciton trap sites are emissive, such as the anthryl defect sites in **P10** and **P11**, then they can dramatically alter the emission spectra of CPs in their film state.

To further investigate the effects of exciton migration on luminescence properties, absorption and fluorescence spectroscopy were conducted on PPE solutions in various degrees of aggregation. By adding a poor solvent (i.e., a solvent in which **P10** is in a collapsed or aggregated state) to a PPE solution dissolved in a good solvent (i.e., a solvent in which the polymer is in an expanded and well-dissolved state), one can study the polymers in various degrees of aggregation. In dilute tetrahydrofuran (THF) solution, **P10** was well dissolved and individual polymer chains were isolated; therefore, only *intra*chain exciton migration is possible and the small concentration of emissive exciton traps was not noticeable in the fluorescence spectra. Thus, THF solutions of **P10** appear fluorescent blue, as characterized by the sharp emission band around 432–434 nm. However, in a 50:50 THF:H_2O cosolvent mixture, **P10** was present in the aggregated state, held together by hydrophobic and π–π interactions. Upon aggregation, *inter*chain exciton migration became significant, so the emissive exciton traps noticeably altered the fluorescence spectra, exhibiting a dominant green emission band around 513 nm. If the ratio of the anthryl comonomer in **P10** is increased, the ratio of green to blue emission (I_{green}/I_{blue}) in the aggregated state also increases.

Furthermore, the fluorescence color change of **P10** dispersed in a solid poly(vinyl alcohol) (PVA) matrix was investigated. PVA is a water-soluble polymer that has been widely used to make water-permeable hydrogels. In order to disperse **P10** in PVA, a THF solution of **P10** was quickly added into an aqueous solution of PVA and the resulting, precipitated polymer blend was crosslinked with glutaric dialdehyde before isolation. Upon washing the **P10**/PVA blend with THF, it became fluorescent blue and remained so even after drying. Subsequently, submerging this blend into pure water for 2 min causes it to become fluorescent green. The observed blue-to-green fluorescence color change was attributed to the water-induced aggregation of the PPE chains within the PVA matrix. Surprisingly, rewashing this fluorescent green blend in THF did not restore blue fluorescence – this was probably due to the difficulty of separating individual PPE chains once they become strongly aggregated in 100% water.

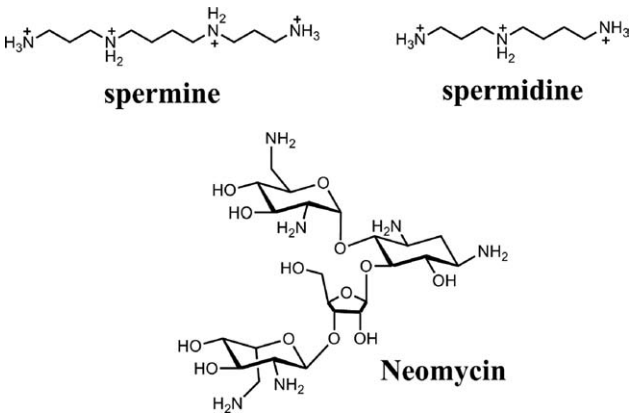

FIGURE 10 Structures of (a) spermine, (b) spermidine, and (c) neomycin.

The phenomenon of enhanced exciton trapping in PPE aggregates was exploited to make aggregation-based sensors for nonquenching multicationic analytes.[16] Nonquenching analytes are described as analytes that cannot participate in direct quenching of the inherent fluorescence intensity of a CP via electron transfer or energy transfer due to incompatible redox and spectral properties, relative to the photoexcited CP. Examples of such analytes are biologically relevant small-molecules, such as multicationic spermine and spermidine, and neomycin (see Fig. 10). It was found that spermine, spermidine, and neomycin induced the formation of tightly associated aggregates in ethanol solutions of the polyelectrolyte **P11**, which was accompanied by a visually noticeable blue-to-green fluorescence color change (Fig. 11). Dicationic and monocationic amines were not observed to affect this change, thus demonstrating that a conjugated polyelectrolyte sensor relying on nonspecific, electrostatic interactions may still attain a certain level of selectivity.

Although CP aggregates represent another option to enable 3D exciton migration (other than thin films), it must be noted that, with few exceptions, the strong electronic interactions between chains of CPs that accompany aggregation dramatically lower their quantum efficiency. This is due to the phenomenon of self-quenching, which can be generally described as any interaction between an excited molecule, M^*, and a ground-state molecule of the same type, M, that leads to fluorescence quenching of M^*.[17] Therefore, it is generally true that the design principles for maintaining high quantum yields in CPs have been diametrically opposed to those for the optimization of charge and exciton transport, which encourage greater interpolymer contact.[18,19]

However, it *is* possible to produce strongly interacting polymer chains with 3D electronic interactions while maintaining high luminescence efficiency (Fig. 12). Specifically, it has been proposed that an oblique orientation between neighboring transition dipole moments of CPs will prevent self-quenching.[20] Based on an exciton-coupling model, a parallel

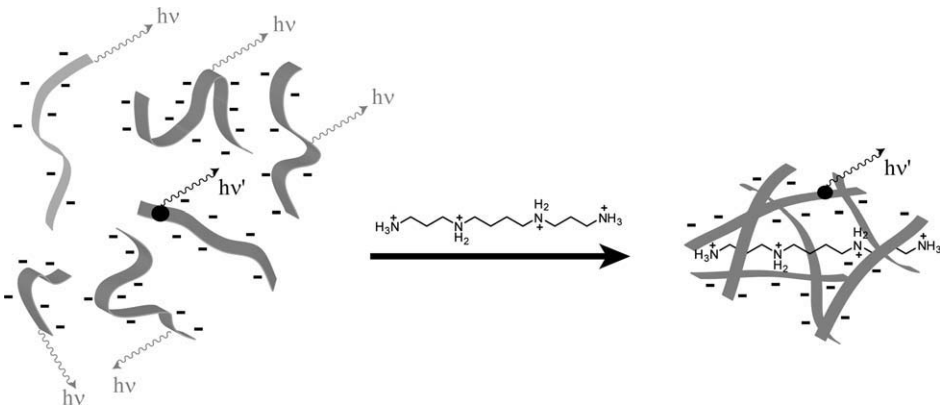

FIGURE 11 Schematic description of aggregation-based sensors for nonquenching, multicationic analytes. Adapted with permission from ref. 16. Copyright 2007 American Chemical Society.

orientation of polymer chains is expected to result in cancellation of transition dipoles to give a forbidden S_0–S_1 transition, but coupled chromophores with oblique organizations should exhibit an allowed S_0–S_1 transition.[21] Therefore, by incorporating specific chemical structures within the repeat unit of a CP that enforce an oblique arrangement of chain segments, highly luminescent CP aggregates can be accessed. Following this concept, we will describe two PPE systems that exhibit a highly emissive aggregated phase and discuss the role of specific chemical structures in enabling oblique packing of chromophores.

Pentiptycene (see Fig. 13) displays a rigid, 3D structure, which, upon inclusion within a CP backbone, effectively prevents π-stacking or excimer formation between individual chains.[18] In comparison with analogous PPEs lacking a pentiptycene comonomer, thin films of **P13** display enhanced fluorescence quantum yield and stability. Moreover, thin films of **P13** exhibit exceptionally high sensitivity as artificial fluorescent chemosensors for the vapors of nitroaromatic compounds, such as TNT and 2,4-dinitrotoluene (DNT).[12] Essentially, the pentiptycene moiety imparts a porosity to solid-state structures [Fig. 13(c)] that prevents direct electronic interaction between polymer chains (thus inhibiting self-quenching) while still allowing for strong dipole–dipole interactions (thus enabling 3D exciton migration).

Given the rigid structure of pentiptycene-incorporated PPEs, however, it was not initially anticipated that oblique aggregates of such polymers could be formed. Therefore initial investigations[22] into fabricating obliquely aligned PPE aggregates were carried out with **P14**. Chiral side chains were introduced into the repeat unit with the expectation that chirality, coupled with the normal twisting of polymer backbones, will yield self-assembled, ordered aggregates. Although enantiomerically pure **P14** was found to initially form chiral aggregates in 40% methanol/chloroform [see Figs. 14(a)–(c)], the fluorescence intensity of these aggregates was strongly decreased relative to isolated polymer chains in dilute chloroform solutions. Moreover, the preliminary chiral structures thus formed ultimately rearranged to favor a stronger aggregate with coincident alignment of polymer chains at methanol concentrations higher than 50%. The resultant organization gave a low or nonexistent dihedral angle between polymer chains and, as expected, the fluorescence quantum yield dropped to $<5\%$ of its original value.

Therefore, in order to stabilize a strongly aggregated chiral and emissive organization of polymers while preventing aggregated chains from achieving a collinear structure, pentiptycene-containing structures were investigated.[22] Although pentiptycene-containing PPEs were not expected to form

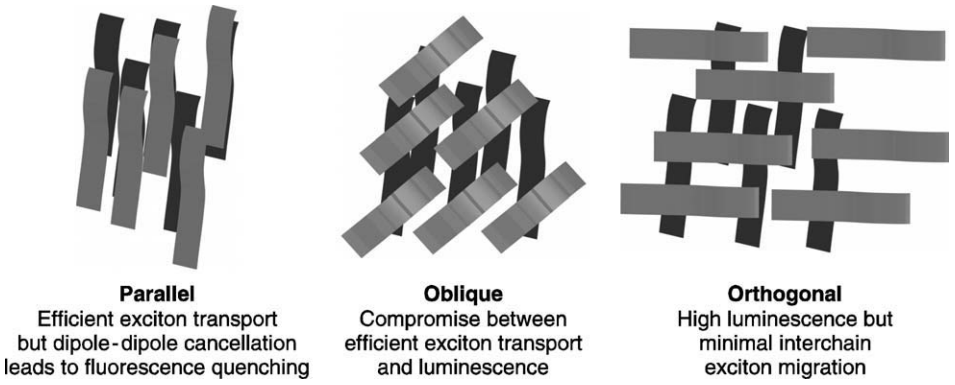

FIGURE 12 Three possible orientations of strongly interacting polymer chains and their corresponding optical and charge-transport properties.

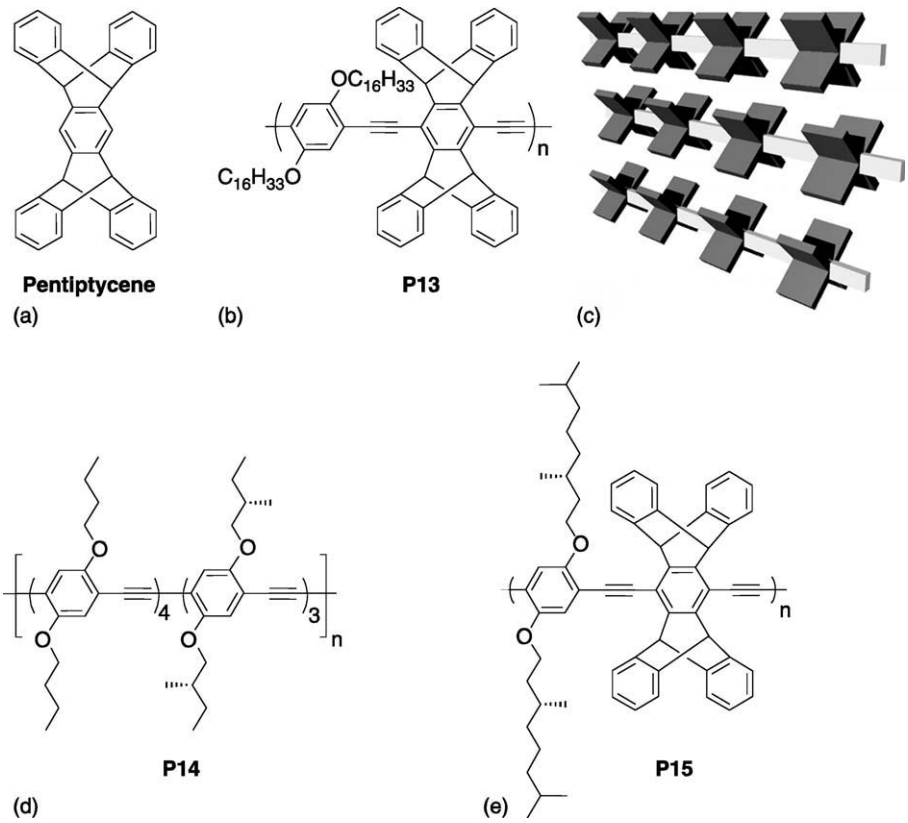

FIGURE 13 (a–c) Structures of pentiptycene, a pentiptycene-incorporated PPE and a simplified representation of the three-dimensional structure of pentiptycene-incorporate PPEs. (d,e) Structures of two PPEs used in aggregation studies.

aggregates, it was initially found that addition of methanol (30%) to solutions of **P13** yielded aggregates with significantly quenched emission ($\Phi = 0.21$). These aggregates were much slower to assemble than those of **P14** and it was hypothesized that the polymer chains assemble into an interlocking structure, in which the polymer chains are constrained in the clefts between the pentiptycene groups [see Figs. 14(d)–(f)]. Considering that such an interlocking structure would prevent a coincidence of strongly interacting polymer chains, the aggregation behavior of an enantiomerically pure, pentiptycene-containing PPE, **P15**, was investigated. On the basis of solvent-dependent circular dichroism and absorbance spectroscopy, **P15** was indeed found to form restricted chiral aggregates in a poor solvent (methanol) yet still retaining the majority of its fluorescence intensity ($\Phi = 0.61$).

This unique aggregated state of P15 also showed sensitivity enhancements toward nitroaromatics. In solutions, fully aggregated **P15** was 15-fold more sensitive to fluorescence quenching by TNT and DNT than fully solvated **P13**. In addition, spun-cast films of aggregated **P15** displayed a fourfold increase in sensitivity toward TNT vapor (75% fluorescence quenching within 10 s) over optimized thin films of **P13**. The increased sensitivity of the fluorescent, chiral aggregates is proposed to derive from both an improved exciton diffusion length in the 3D-coupled chiral grids and an extension of the polymer conjugation length in the highly organized aggregated structure.

In addition to pentiptycene moieties encouraging an oblique packing of PPE chains, other 3D structures, such as cyclophanes, were also found to yield emissive PPE aggregates.[23] Specifically, spun-cast samples of polymer **P16** (Fig. 15) displayed a visible, strong yellow emission that could be assigned to fluorescence from aggregated main chains. Notably, **P16** has a very low solution fluorescence quantum yield ($\Phi = 0.06$) due to electron transfer quenching of the polymer excited state by the amine residues. However, the aggregated phase of **P16** has a quantum yield 350% ($\Phi = 0.21$) of its solution value. This observation is unique because most other examples of CP aggregates display fluorescence quantum yields that either match (at best), or are only a few percent of the solution values. In this case, it is likely that the system displays a disordered structure and that isolated oblique aggregates are a minority species. The strong emission is a result of the fact that these aggregates are low-energy species and that energy migration results in a disproportionate emission intensity.

Kinetics of Energy Migration in Thin Films

In order to ascertain the photophysical and energy transport properties of PPEs, highly aligned LB multilayers of **P2** that were surface modified with luminescent traps (acridine orange, AO) were fabricated and investigated.[24] The LB deposition technique produced highly anisotropic films of **P2** with a well-defined thickness. The film thickness increases linearly with the number of layers transferred, thereby

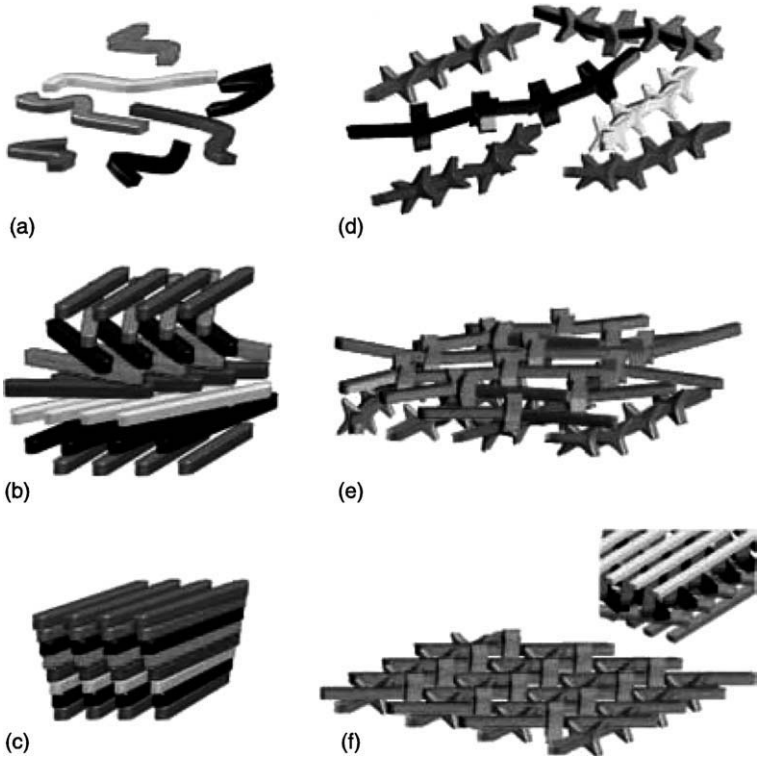

FIGURE 14 (a–c) Representation of the solution aggregation behavior of **P14** with increasing methanol concentrations. (d–f) Representation of the solution aggregation behavior of **P15** with increasing methanol concentration. Top: **P14** (a) and **P15** (d) dissolved in neat chloroform. Both polymers are highly solvated and there are no interactions between polymer chains. Middle: Aggregation of **P14** occurred and the rigid-rod PPEs form a lamella structure within each plane (b). The chiral side chains guide the polymers into a chiral macrostructure as depicted. The formation of the optically active macrostructure is guided by the influence of the chiral side chains. Polymer **P15** aggregates analogously to **P14**, but because of the presence of the pentiptycene groups, a slightly irregular interlocked structure results (e). The macrostructure of **P15** is shown in a two-layer graphic for simplification and clarity. Bottom: The initial chiral macrostructure of **P14** has been "untwisted" (c), which is favorable as it maximizes π–π stacking in the edge-on conformation. The dihedral angle assumes a very small value, affording a very weak dichroic signal and low fluorescence quantum yield. Polymer **P15** self-assembles into a tighter structure (f) by incorporating the polymer into the clefts of the pentiptycene groups. Because the "untwisting" motion observed in **P14** is hindered, **P15** is able to maintain its optically active structure and its high fluorescence quantum yield. The inset illustrates the anticipated chiral gridlike structure. Reprinted with permission from ref. 22.

producing a well-defined geometry and distance for which to study energy migration processes.

The fact that energy migration is present in **P2** could be readily seen in wavelength-dependent lifetime measurements on spin-cast films. The excited-state lifetime was observed to increase when monitored at progressively longer wavelengths (λ = 460, 475, and 495 nm). These lifetime characteristics are consistent with a model that describes the polymer as a continuous distribution (usually Gaussian) of site energies. In this model, each state corresponds to a CP segment that is interrupted by chain defects (conformational or chemical), with the longer segments having lower energy, and energy migration is described as incoherent hopping of excitations to lower energy states. Emission from high-energy states (i.e., shorter wavelength of emission) should exhibit a faster decay rate due to energy transfer to lower energy chromophores within the system, consistent with what was observed for spin-cast films of **P2**. Evidence for intrachain energy migration in **P2** is likewise provided by fluorescence depolarization measurements, which will be discussed in a later section.

Emissive trapping sites were deposited selectively on the film surfaces by dipping LB films into methanol solutions of

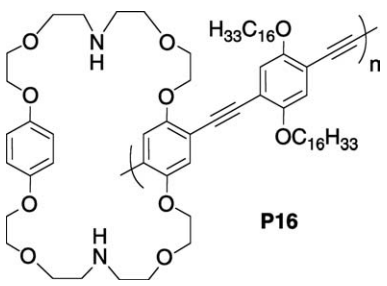

P16

FIGURE 15 Structure of a PPE that forms a highly emissive aggregate.

AO, which was chosen because its emission and absorption spectra are well separated from those of **P2** and its absorption spectrum has good overlap with the emission of **P2**. Additionally, the solubility of AO was almost orthogonal to that of **P2**, which allowed LB films of **P2** to be dip-coated in solution of AO with varying concentrations. AO was found to selectively localize at the film's surface, as evidenced by the fact that the ratio of AO fluorescence intensity between films of different thicknesses examined immediately after dipping or after extended periods of time remained constant. Polarization measurements showed that the AO transition dipole was principally aligned parallel to the polymer chain.

In the simplest case of energy transfer to AO from a monolayer of **P2**, the average lifetime of an excitation (τ) in an infinite 1D chain with randomly distributed efficient quenching traps should be $\tau = 1/(2WC^2)$, where C is the trap concentration and W is the hopping rate between neighboring sites. Therefore, the steady-state transfer rate should be proportional to C^2. In contrast, it was found that the degree of energy transfer to AO traps from a monolayer of **P2** was linearly dependent on the concentration of AO. This observation can be explained by either 1D energy migration with inefficient trapping or 2D transport. Considering that monolayer films of **P2** organize into highly aligned structures that could potentially allow excitations to undergo efficient interpolymer energy transport, the latter explanation of 2D transport is more likely.

If the number of LB layers was varied, an increase in the AO emission with increasing polymer layers was observed, up to 16 layers. At low concentrations of the AO trap, the AO fluorescence had a linear dependence on AO concentration, similar to the monolayer system described above. This last point leads to the conclusion that, at low AO concentration, the steady-state energy transfer rate in a monolayer film is less than $1/\tau$, where τ is the polymer's excitation lifetime. Moreover, the fact that the relative fluorescence of AO increases with increasing numbers of polymer layers is a direct indication of a transition to a 3D energy migration topology. The observation of saturation behavior in films with higher numbers of layers is a manifestation of the diffusion length for energy migration. The increase in the efficiency of energy migration to surface traps with increasing film thickness may, at first glance, seem counterintuitive since the concentration of AO relative to that of **P2** is actually smaller in thick films. However, this increased trapping efficiency is a direct result of the fact that 3D exciton migration necessarily creates a more efficient trapping process.

X-ray measurements on the monolayer and multilayer films revealed that the thickness per layer is 11 Å. Since the bimolecular Förster radius for most organic compounds is 20–60 Å, dipole–dipole excitation transfer between polymers must be involved as part of the mechanism for energy transfer to the AO trap.

In order to model the various energy transfer processes in LB films of **P2** surface modified with AO, rate constants for each possible energy transfer and decay process for an N-layer system were assigned. Figure 16 outlines these rate constants and their associated processes for a three-layer system. Since PPEs have a relatively large band gap and a narrow bandwidth, excitations were assumed to exist as strongly bound excitons. Assuming a steady-state population of all excited species, a set of balanced equations can be formulated (see Fig. 16) and, ultimately, the relative intensity of AO fluorescence versus number of LB layers can be modeled. Such modeling has determined, first, that the rate of energy transfer between layers exceeds 6×10^{11} s^{-1}. This high rate results in a uniform excitation population throughout all the layers of the LB films. Additionally, the model confirms the saturation of AO fluorescence intensity with increasing LB layers.

Therefore, it is clear that an optimal thickness will exist in sensor schemes requiring exciton trapping at the polymer surface. However, it must be pointed out that additional enhancements in energy migration may be possible by creating multilayer structures that provide vectorial energy transport in a specific direction. For example, in the striated, three-component film depicted in Figure 8, energy was preferentially transferred to the surface by utilizing layers of sequentially decreasing band gap and, in this way, the 16-layer energy transfer limitation for PPEs was overcome.

LIFETIME MODULATION

As discussed above, a thorough understanding of the mechanisms underlying energy migration in CPs is necessary to design its enhancement. The high efficiency of energy transfer in most conjugated systems relative to systems with pendant chromophores suggests that strongly coupled electronic intrachain (Dexter-type) processes may increase transport in these systems over those provided solely by the dipole–dipole (Förster-type) interactions that govern weakly interacting chromophores. Discrepancies between the two mechanisms allow the determination of which process dominates in a given system.[25]

As derived by Förster, the dipole–dipole approximation yields a transition probability (k_{ET}):

$$k_{ET} = \frac{\kappa^2 J 8.8 \times 10^{-28}\text{mol}}{n^4 \tau_0 R_{DA}^6} \quad (5)$$

where κ is an orientation factor, n is the refractive index of the medium, τ_0 is the radiative lifetime of the donor, R_{DA} is the distance (cm) between donor (D) and acceptor (A); and J is the spectral overlap (in coherent units cm^6 mol^{-1}) between the absorption spectrum of the acceptor and the fluorescence spectrum of the donor. Therefore, a weakly allowed transition, as manifest in a long radiative lifetime, should discourage purely coulombic energy transfer.

Electron exchange effects contributing to the energy transfer described by Dexter account for shorter range processes that result from direct wavefunction overlap of interacting molecules. In this case, the transition probability is described by

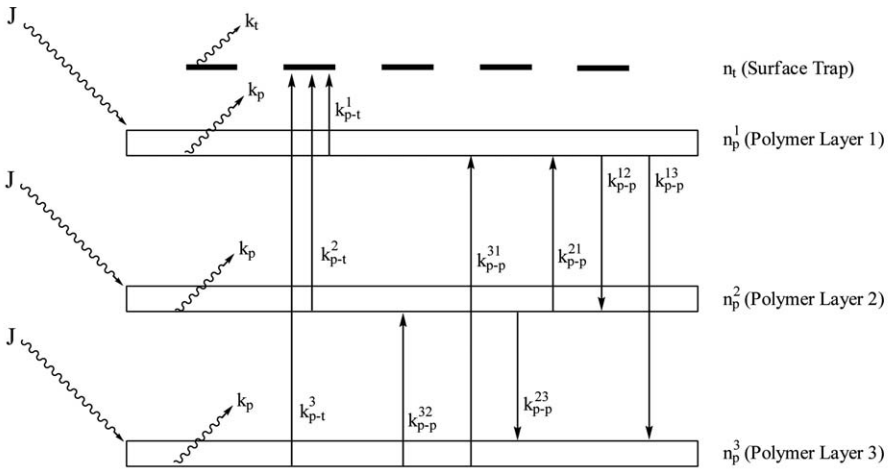

J : Intensity of steady state excitation

$n_{p,t}$: Excitation population in polymer layers and traps

$k_{p,t}$: Decay rates of polymer and trap. $k_P = 1/\tau_P$, $k_t = 1/\tau_t$

k^1_{p-t} : Rate constant for energy migration from polymer layer 1 to the trap. $k_{p-t} \sim C$, where C is the concentration of traps.

$k^{2,3}_{p-t}$: Rate constant for direct energy transfer to the trap from polymer layers 2 and 3. $k^2_{p-t} \sim \frac{C}{\ell^6}$, $k^3_{p-t} \sim \frac{C}{(2\ell)^6}$
ℓ is the thickness of the layer

k^{ij}_{p-p} : Rate constant for energy transfer between polymer layers i and j $k^{ij}_{p-p} \sim \frac{1}{(\ell(i-j))^6}$

A steady state assumption for n_t, n^1_p, n^2_p, and n^3_p gives:

$$-n_t k_t + n^1_p k^1_{p-t} + n^2_p k^2_{p-t} + n^3_p k^3_{p-t} = 0$$

$$-n^1_p k_p - n^1_p k^1_{p-t} - n^1_p k^{12}_{p-p} - n^1_p k^{13}_{p-p} + n_p k^{21}_{p-p} + n^3_p k^{31}_{p-p} + J = 0$$

$$-n^2_p k_p - n^2_p k^2_{p-t} - n^2_p k^{21}_{p-p} - n^2_p k^{23}_{p-p} + n^1_p k^{12}_{p-p} + n^3_p k^{32}_{p-p} + J = 0$$

$$-n^3_p k_p - n^3_p k^3_{p-t} - n^3_p k^{32}_{p-p} - n^3_p k^{31}_{p-p} + n^1_p k^{13}_{p-p} + n^2_p k^{12}_{p-p} + J = 0$$

FIGURE 16 Schematic representation and rate constants for a three-layer Langmuir–Blodgett assembly of **P2** with an emissive trap (acridine orange) placed at the film surface. The equations resulting from a steady-state excitation population of the layers and the trap are shown. Adapted with permission from ref. 24. Copyright 1999 American Chemical Society.

$$k_{ET} = KJ \exp(-2R_{DA}/L) \quad (6)$$

where K is related to specific orbital interactions, J is the spectral overlap, R_{DA} is the donor–acceptor distance, and L is the van der Waals radii distance between donor and acceptor. This process is often termed electron exchange because molecules must be almost within the van der Waals radii of each other to interact. In the specific case of CPs, chromophores are directly conjugated and, therefore, one might expect the Dexter mechanism to dictate the overall efficiency of energy migration, at least within the polymer backbone.

To determine the dominant *intra*chain energy migration mechanism in PPEs, the unique oscillator strength independence of the Dexter mechanism was invoked to guide the design of polymers with long radiative lifetimes. Long radiative lifetimes translate into reduced oscillator strengths of D* to D and A to A* transitions, which, according to the Förster mechanism [eq (5)], would result in a severely truncated rate of energy transfer. However, because the Dexter electron exchange mechanism does not depend on the oscillator strength, longer lifetimes affected by less allowed transitions can serve to increase energy transfer by providing more time for the excitation to migrate before radiative decay.[25]

Triphenylene-Incorporated PPEs

Long-lifetime PPEs can be accessed by incorporating structures with extended aromatic cores, such as triphenylene, dibenzo[*g,p*]chrysene and benzothiophene, into the backbone of the polymer. Triphenylene has a well-known symmetrically forbidden ground-state transition and, therefore, exhibits a long excited-state lifetime. Although incorporation into a CP will decrease the triphenylene's symmetry, it was hypothesized that the strong aromatic structure would dominate the photophysics of the resulting polymer. In order to determine the general effect of triphenylene incorporation, a family of triphenylene-based poly(*p*-phenyl ethynylene) s (TPPEs) was synthesized along with chemically similar phenylene analogs (see Fig. 17).[26] Polymers were size-selected by gel permeation chromatography to ensure comparison of

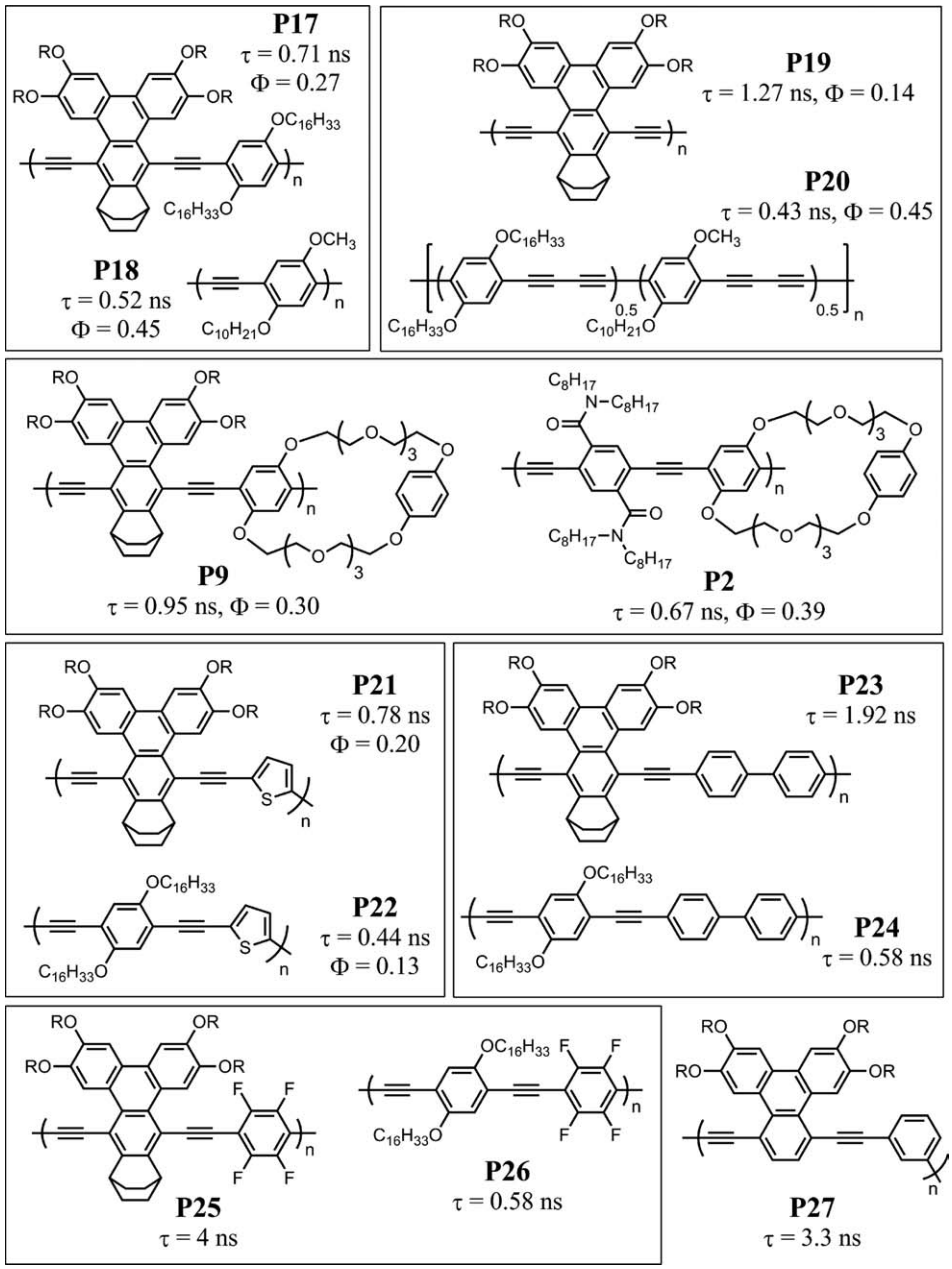

FIGURE 17 Structures of triphenylene-incorporated PPEs and their corresponding phenylene PPEs, and the photophysical properties of all polymers considered.

similar chain lengths and the excited-state lifetimes were measured in the frequency domain in methylene chloride solutions. It was found that triphenylene incorporation universally extended the excited-state lifetime of targeted PPEs without severely compromising quantum yield. The combination of Φ and τ data demonstrate that the enhanced lifetimes are principally due to differences in radiative rates and not differences in nonradiative rates.

In PPEs where the excitation is more localized, the lifetime-enhancing effect of the triphenylene moiety was more pronounced. An example is **P23**, consisting of a triphenylene monomer and a biphenyl monomer. Because biphenyl planarizes in the excited state, a large Stokes shift is observed in the resulting polymer. This process serves to localize the excitation and the radiative decay rate becomes more competitive with energy transfer. Consequentially, the lifetime of **P23** is about three times longer than its phenylene analog, **P24**. This effect is also observed in *meta*-linked PPE, **P27**: the *meta* linkage disrupts conjugation, thus localizing the excitation and resulting in one of the longest lifetimes observed for TPPEs. As expected, PPEs with a larger triphenylene component demonstrated more pronounced lifetime enhancement relative to their phenylene analogs (**P19** vs. **P20**).

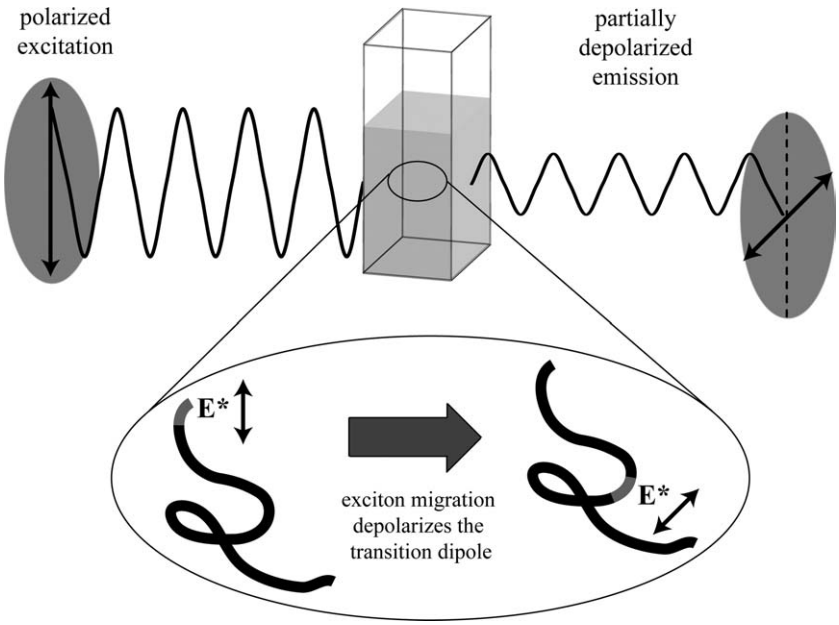

FIGURE 18 A simplified pictorial of depolarization due to energy migration in conjugated polymers (CPs). The excitation beam is vertically polarized and therefore only vertical transition dipoles are initially excited on the CP chain. Vertically polarized excitons on the polymer chain migrate. As they move over a disordered polymer chain, they lose their initial polarization. Thus, the emission of the polymer is depolarized relative to the excitation beam. This amount of measured depolarization directly indicates the extent of energy migration in the CP. Adapted with permission from ref. 25, Rose et al. 2007.

In addition, electrostatic variation in TPPEs was found to lead to excited-state interactions. The long lifetime (4 ns) observed for **P25** most probably arises from an exciplex that is formed between the triphenylene moiety and its electron-deficient tetrafluorinated comonomer. This proposal is also supported by the broad, red-shifted emission spectra recorded for **P25**. Notably, these features were not observed for the phenylene analog, **P26**, thus suggesting that the flat, electron-rich nature of the triphenylene is necessary to induce exciplex formation.

The relationship between excited-state lifetime and energy migration can be investigated through fluorescence depolarization measurements.[25] A simplified pictorial depiction of depolarization due to energy migration in CPs is shown in Figure 18. The excitation beam is vertically polarized and, therefore, only vertical transition dipoles are initially excited on the CP chain. Vertically polarized excitons on the polymer chain can migrate and, as they move over a disordered polymer chain, can lose their initial polarization. The emission of the CP is thus depolarized relative to the excitation beam. Therefore, the amount of measured depolarization directly indicates the extent of energy migration in the CP.

Since all polymers studied were high molecular weight materials, they can be considered rotationally static over the emission lifetime of the polymer. Therefore, energy migration is the major contributor to the fluorescence depolarization in CPs, and the exciton loses more of its initial polarization as it diffuses along a disordered polymer chain. The polarization value, *P*, was determined from the standard equation

$$P = \frac{I_{\parallel} - GI_{\perp}}{I_{\parallel} + GI_{\perp}} \tag{7}$$

where $I_{||}$ and $I_{\perp}$ are the intensities of emissions detected parallel and perpendicular to the polarization vector of the incident light, respectively, and G is an instrumental correction factor. Theoretically, the highest value of P for a randomly oriented, isolated, fixed chromophore with coincident transition dipoles for absorption and emission is 0.5.

Concurring with lifetime data, depolarization was found to be universally more pronounced in TPPEs than their phenylene analogs [Fig. 19(a)]. In the case of polymers **P21** and **P22**, the kinked thiophene linkage resulted in a much greater depolarization than in other polymers studied. Greater polarization loss per migration step is expected in a kinked structure. Polymer **P27**, with its localizing biphenyl monomer, retained one of the highest polarization values [Fig. 19(b)]. Polymer **P25**, however, displayed the highest polarization value among the TPPEs. The energy minimum formed by its exciplex probably quickly traps the wandering excitation, thus reducing energy migration.

Additionally, the fluorescence depolarization of a subset of polymers as a function of excitation energy was studied in order to separate depolarization owing to energy migration from that due to absorption/emission dipole alignment [Fig. 19(b)]. If energy migration is indeed present, then polarization values should decrease as excitations move to shorter wavelengths. Measurements were performed on materials selected for similar chain length, all above the small molecular weight regime. As excitation energy is increased, it was found that both the

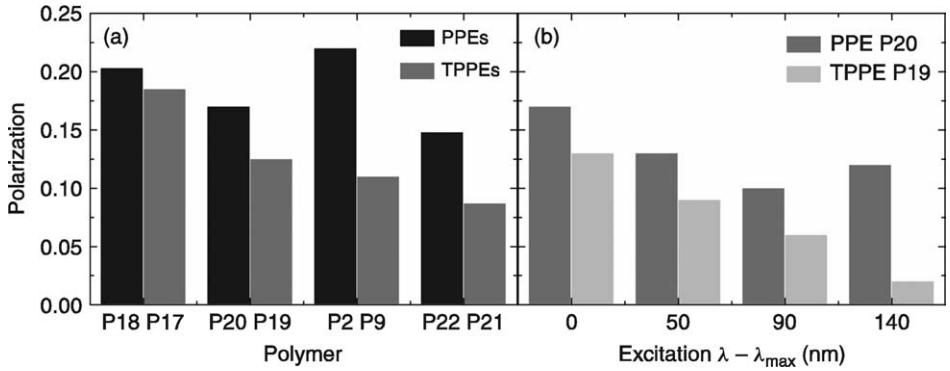

FIGURE 19 Polarization values for a family of TPPEs and their corresponding PPEs. Gray bars are polarization values for TPPEs and black bars are polarizations for PPEs. Both are excited at λ_{max} and in every instance, TPPEs exhibit greater depolarization, indicating more extensive energy migration. Adapted with permission from ref. 26. Copyright 2001 American Chemical Society.

TPPEs and their phenylene analogs display lower *P* values, consistent with population of higher energy excitons that readily lower their energy by migration to lower energy states. However, polarization continued to significantly decrease with shorter wavelengths of excitation in TPPEs but only leveled off in PPEs, indicating that radiative rates of emission are not competitive with energy migration in TPPEs as they are in PPEs. If the Förster mechanism dominated, then the enhanced radiative rates in PPEs would encourage more extensive energy migration (and therefore greater fluorescence depolarization) as compared to the TPPEs; however, the opposite phenomenon is observed, thus lending credence to the claim that the Dexter mechanism is the dominant intramolecular energy transport process in these systems.

Chrysene-Incorporated PPEs

It was also possible that the increased fluorescence depolarization observed for the TPPEs is due to a reduced persistence length as compared to analogous PPEs (see Fig. 20). Steric interactions between the ethynylenes and proximate CH bonds of the TPPEs could conceivably result in a more coiled structure that could be responsible for the more rapid fluorescence depolarization in the TPPEs. To address this concern, polycyclic dibenzo[*g,p*] chrysene-based poly(*p*-phenyl ethynylene)s (CPPEs) were investigated (Fig. 21).[27] CPPEs lack any complicating steric factors and have a more rigid structure that should increase the persistence length and yield less coiled polymers compared to PPEs.

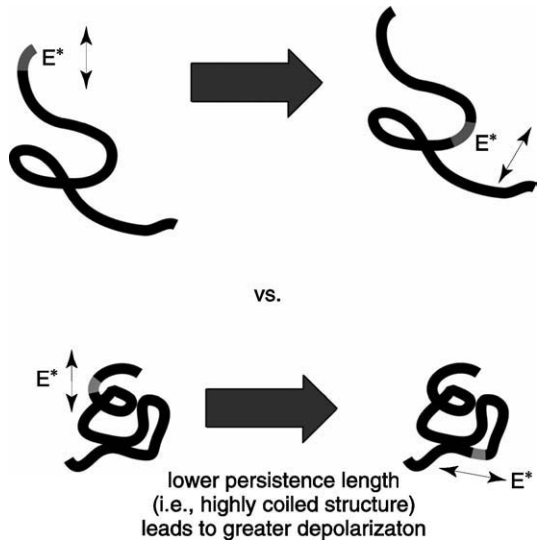

FIGURE 20 Possible persistence-length dependence of fluorescence depolarization.

The photophysical properties of the CPPEs were found to be similar to those observed in TPPEs: that is, longer excited-state lifetimes and more extensive energy migration. Polymers **P29** and **P31** displayed lifetimes greater than 2 ns, while most PPEs have sub-nanosecond lifetimes. Polarization studies confirmed the presence of enhanced exciton migration in CPPEs.[25] For all chain lengths and at all excitation wavelengths, the polarization values of CPPEs were about half of those in the corresponding PPEs. Additionally, polarization data as a function of excitation wavelength discounted dipole displacement as a main contributor to depolarization. Chain length dependent studies on **P29** revealed that radiative decay did not supersede energy migration even for the longest chain lengths ($n \sim 220$). Therefore, the CPPEs, similar to the TPPEs, allowed for greater intrachain exciton migration than PPEs because of the fact that energy migration is not truncated by radiative deactivation of the excited state.

Thiophene-Based Model Compounds and PPEs

Lastly, polymers with pendant thiophenes further illuminate lifetime extension (Fig. 22).[28] Sulfur incorporation benefits materials properties in part owing to the larger radial extension of its bonding. This promotes cofacial electronic interactions between stacked molecules that could enhance energy transfer. Cyclized and noncyclized versions of each model compound and polymer were investigated to assess the effects of imposed symmetry and rigidity on the photophysics of the material. With both *meta* and *para* linkages represented, the family of polymers investigated allowed for

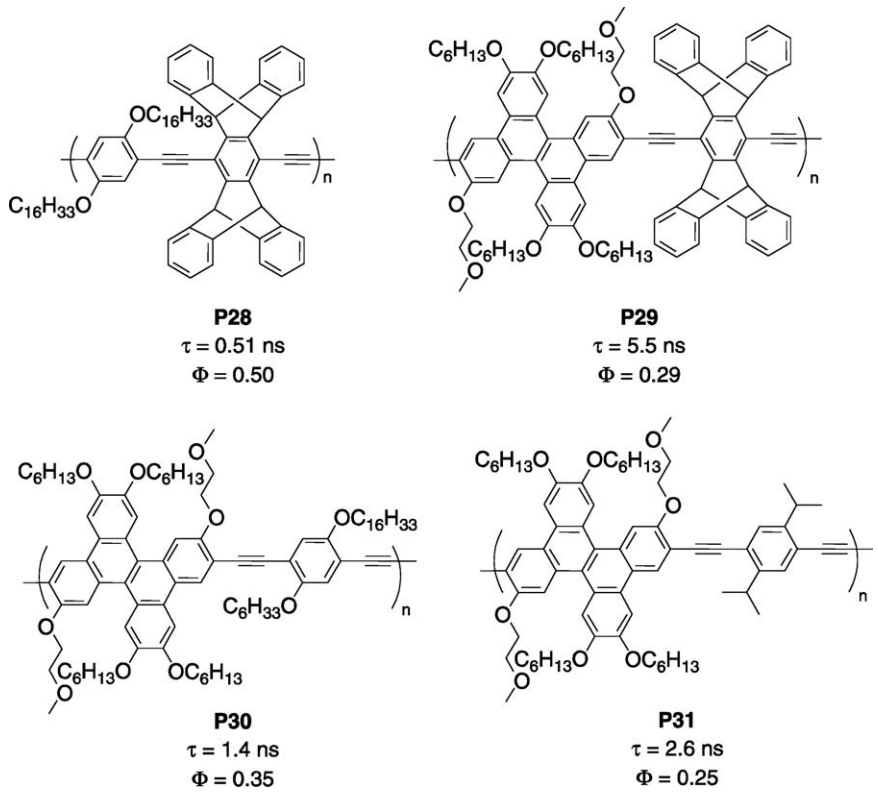

FIGURE 21 Structures of chrysene-incorporated PPEs.

exploration of the effects of different degrees of aromatization as well as changes in conjugation pathways.

To predict the behavior of such thiophene-containing polymers, model compounds **MC1–4** provided systems with precisely defined conjugation lengths, allowing separation of planarization effects from effective conjugation-length variations. The cyclized compounds **MC2** and **MC4** showed a sharpening of vibronic structure concomitant with a decrease in Stokes shift as degrees of freedom were reduced. The oscillator strength of the (0,0) transition was significantly reduced in the *meta* system **MC4** ($\log \varepsilon = 3.63$) when compared with the *para* isomer **MC2** ($\log \varepsilon = 4.69$). Accordingly, *meta* **MC4** had a longer excited-state lifetime (5.00 ns) than the *para* **MC2** (1.12 ns).

While a sharpening of emission spectra was observed, no significant wavelength shift in either system occurred upon cyclizing (aromatizing) either **MC1**–**MC2** or **MC3**–**MC4**. This suggested that there is planarization in the excited state of **MC1** and **MC3** to allow for greater delocalization. Additionally, the lifetime of the both systems was found to increase upon cyclization: the *meta* system displayed a ninefold increase in excited-state lifetime upon cyclization (0.58 ns for **MC3** to 5.0 ns for **MC4**) while the *para* system showed a more modest increase (0.8 ns for **MC1** to 1.12 ns for **MC2**).

Consistent with other CPs, the photophysical properties of the model compounds **MC1–4** were reflected in the corresponding polymers. The absorption spectra of rigid, aromatized **P33** and **P35** displayed sharper vibronic structure and a decrease in Stokes shift when compared with the noncyclized **P32** and **P34**. The *meta*-cyclized polymer **P35** displayed much lower oscillator strength at the band edge than its *para* analog, **P33** – which was predicted by the corresponding model compounds. Aromatization effects only slightly shifted the emission maxima of both the *meta* and *para* systems. As in **MC1** and **MC3**, this may attest to excited-state planarization in the flexible systems.

Lifetime trends in the model compounds were also consistent with the related polymers. In accordance with the diminished oscillator strength, the *meta* polymers **P34** and **P35** displayed a lifetime discrepancy (0.30 vs 1.06 ns, respectively) similar to that of their model compounds, **MC3** and **MC4** (0.58 vs 5.00 ns, respectively). The *para* polymers also mimicked the model systems. However, in this case, the model compounds **MC1** and **MC2** exhibited comparable lifetimes (0.80 vs 1.12 ns, respectively) before and after cyclization. As a result, the *para* polymers shared almost identical lifetimes (**P32**: 0.57 ns, **P33**: 0.61 ns). Both these examples correspond to the previously observed trend, which suggests that monomer photophysics critically influences the photophysics of the resulting polymers.

Polarization experiments revealed that energy migration is not enhanced without lifetime enhancement[25]. In other words, the *meta*-cyclized polymer **P35** displayed the greatest fluorescence depolarization, with polarization values reaching near zero. This was due to both the enhanced lifetime of the polymer and the curved architecture of the polymer

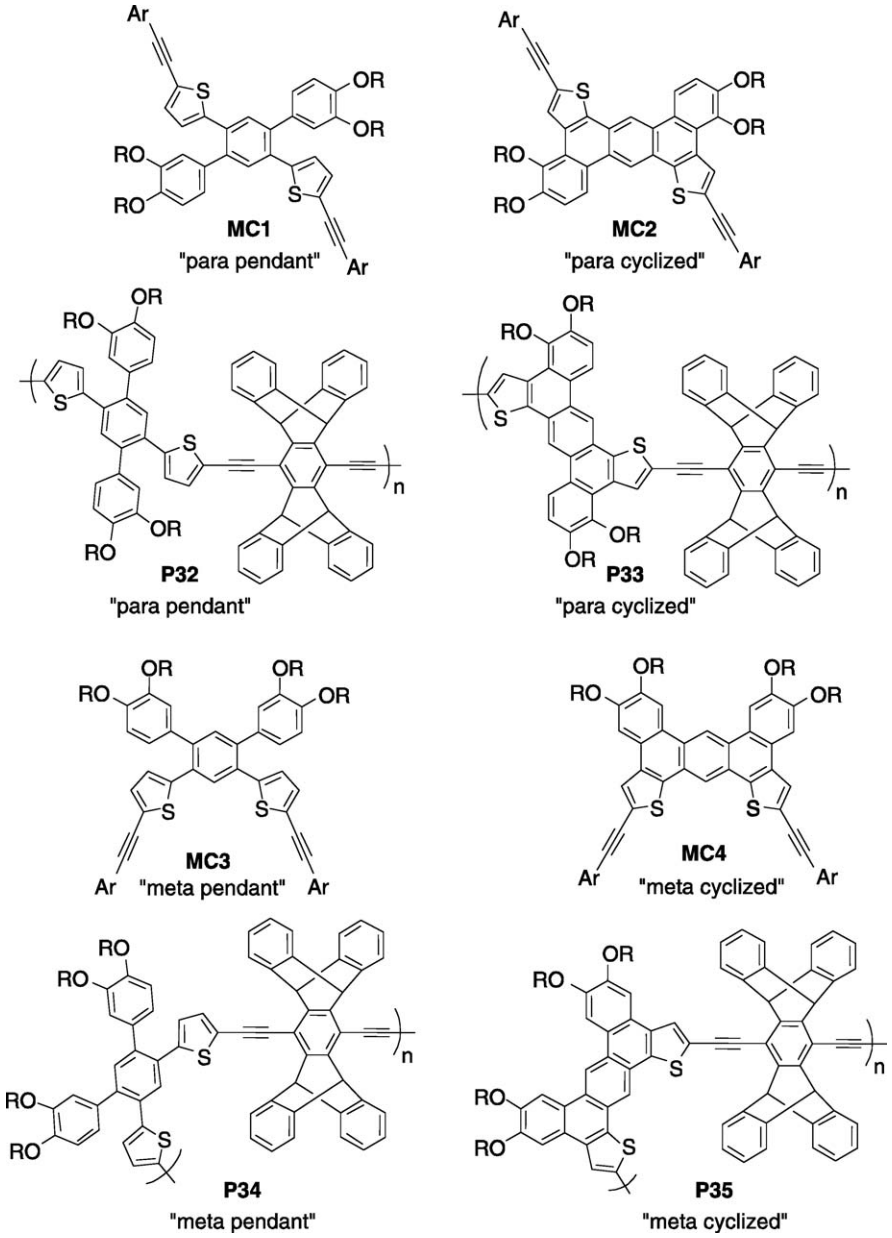

FIGURE 22 Structures of thiophene-based model compounds and PPEs.

chain, which causes significant depolarization even when energy has migrated through a single hop. In contrast, since a large lifetime enhancement was not obtained upon aromatizing the *para*-pendant polymer **P32** to its cyclized analog, **P33**, a large depolarization was not observed for either of the two *para* polymers. Together, the polarization measurements on these thiophene systems underscore an important distinction: simply rigidifying the polymer backbone is not enough to extend lifetime and enhance energy migrations. One must carefully consider chromophore photophysics when attempting to impart these properties into CPs because the excited-state behavior of polymers is essentially encoded by the choice of monomers.

CONFORMATIONAL DEPENDENCE ON ENERGY MIGRATION: CONJUGATED POLYMER – LIQUID CRYSTAL SOLUTIONS

The achievement of complete control over the conformation of CP single chains and their assembly into functional structures is paramount to the thorough understanding and optimization of energy transfer and conductivity in CPs. Inconveniently, high molecular weight PPEs have finite persistence lengths and exist as flexible coils (as opposed to rigid rods) in solution.[11] Consequently, the disorder displayed in solution is often transferred to the solid-state structures of PPEs, and there is a general lack of long-range molecular order

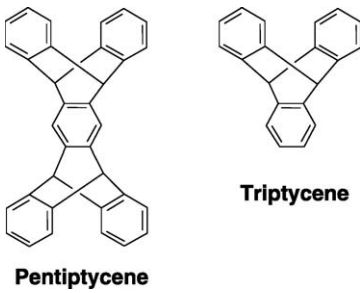

FIGURE 23 Common iptycene scaffolds.

due to conformational disorder in the polymer main chain. The many structural defects in the solid state ultimately result in diminished electronic delocalization and limit the ability to study the intrinsic properties of these materials.

As one potential solution to this conundrum, liquid crystals (LCs) represent an ideal means to produce ordered arrays of molecular wires. Columnar LCs with extended aromatic cores have long been considered 1D conductors; however, there is limited electronic coupling between aromatic cores due to limited overlap of the π-orbitals, particularly in the liquid crystalline state.[29] An alternate strategy to exploit the long-range order of LCs and assemble electronic materials is to dissolve CPs into an LC host. In this way, the strong intramolecular electronic coupling of the CP and the organizational ability of the LC host can work together to form a highly organized electronic material.

Revisiting the rigid, 3D pentiptycene scaffold mentioned earlier, it is worth noting that the 3D nature of pentiptycene and its analog triptycene (Fig. 23) also has important organizational influences. Specifically, the addition of triptycene moieties into the backbone of a polymer can either be used to redirect[30] or enhance[31] molecular alignment in LCs and stretched polymers. This property results from the natural tendency of host–guest mixtures to lower their energy by minimizing the amount of free volume. Therefore, fluorescent dyes, PPEs, and PPVs containing triptycene groups can theoretically be aligned along the nematic director in LCs and thus achieve significant ordering with high-order parameters (S) and dichroic ratios (D).[31]

Accordingly, nematic liquid crystalline solutions of the highly emissive, triptycene-incorporated PPV, **P36**, and the triptycene-incorporated PPE, **P37** (Fig. 24) were investigated.[32] Solutions of **P36** and **P37** in **6CHBT** (Fig. 25) were loaded into LC cells with rubbed internal polyimide surfaces that gave a homogenous alignment of the nematic LC. Polarized absorption spectroscopy of these test cells with the polarizers aligned parallel (0°) or perpendicular (90°) to the nematic director were used to calculate the order parameters, S. The liquid crystalline solvent (a wide variety of nematics were acceptable, but **6CHBT** and **5PCH** were primarily used) had the important feature that it created an extended CP chain conformation that was highly aligned (S ranged between 0.7 and above 0.8). Additionally, the polymers were found to have greatly enhanced conjugation lengths in nematic LC solutions. This could readily be observed by comparing the absorption spectra of **P37** in a CH_2Cl_2 solution and an LC solution: **P37** in a LC solvent displayed an absorption spectrum that was red shifted and had a comparatively abrupt band edge relative to its absorption spectrum in a CH_2Cl_2 solution (Fig. 24). Both these features suggest that the CPs' long axes aligned with the director of the nematic LC and that the polymer chains were in a highly extended conformation as opposed to the typical random coil present in isotropic solutions.

Further proof that the polymers formed true solutions in nematic LCs was provided by demonstrating that the polymers could be reoriented with the nematic host by application of electric fields (Fig. 26). Under an applied field (9 V), the nematic director and the polymer backboned aligned normal to surface of the LC test cells. This resulted in a dramatic reduction (75–80%) in the polymer absorption and complete loss of polarization. These results are due to the realignment of the CP's transition dipole (that is coincident with the polymer's long axis) to match the direction of the electric field (normal to the surface of the test cell), which minimized the projection of the transition dipole along the electric vector of the incident light beam. The reorientation

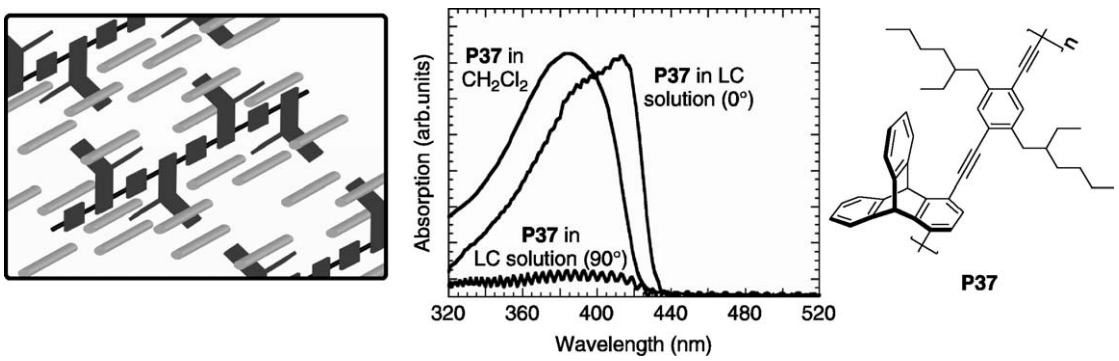

FIGURE 24 Comparison of the absorption spectrum of PPE **P37** in methylene chloride and a nematic liquid crystal solvent (**6CHBT**). The liquid crystal imposes a planarized conformation that is responsible for the steep band edge and red shift of the absorption spectrum. Note that the polarized absorption reveals that the polymer backbone is aligned parallel to the liquid crystal director. Adapted with permission from ref. 32. Copyright 2002 American Chemical Society.

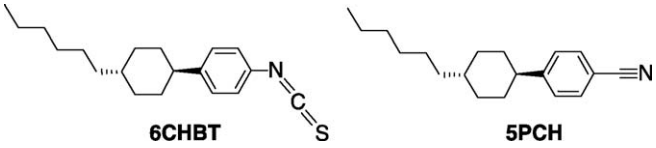

FIGURE 25 Structures of some nematic liquid crystals.

of the CPs was also readily apparent by visualizing the polymer's fluorescence in the presence (fluorescence OFF) and absence (fluorescence ON) of an applied voltage (Fig. 26). In all cases, the polarized fluorescence was rapidly recovered upon removal of the voltage.

To better illustrate the conformational dependence of energy migration in CPs, LC solutions of **P38**, which is a pentiptycene-incorporated PPE end-capped with low-energy anthracene trapping sites, were investigated (Fig. 27).[33] As explained earlier, the introduction of anthracene end groups solicits efficient energy transfer from the polymer backbone to these trapping sites and thus, site-selective, green emission from the polymer termini can be observed if significant exciton migration is operative. Therefore, dissolving **P38** in **6CHBT** allowed for the study of the rate of intrachain exciton migration under conditions of increased conjugation length and high alignment. These studies revealed that the order imposed by the nematic LC solvent increased the energy transfer efficiency to the low-energy anthracene termini. This process was accompanied by a significant increase in the fluorescence quantum yield. The liquid crystalline phase was found to be a necessary requirement for this phenomenon, as when the temperature of the system was increased above the nematic–isotropic transition temperature of the LC host, a dramatic reduction of the energy transfer efficiency and fluorescence quantum yield was observed.

Structure–property relationships that govern the extent of conformational enhancement achievable in PPE–LCs mixtures were investigated using PPEs **P39–41** (Fig. 28).[34] These PPEs contain more elaborate iptycene scaffolds introduced to create polymers displaying greater order and enhanced solubility in LCs at high molecular weights (high molecular weight versions of **P36** and **P37** were found to be poorly soluble in nematic LCs). As expected, **P39** and **P40** displayed higher order parameters ($S_A = 0.86$ and 0.81, respectively) than both **P36** and **P37** ($S_A = 0.69$ and 0.73, respectively). Similar to observations made with **P36** and **P37**, mixtures of **P39** and **P40** in MLC-6884 (which has a negative dielectric anisotropy and a nematic phase at room temperature) displayed the same absorption red-shift and band-sharpening relative to isotropic solutions, thus indicating conjugation-length enhancement in LC solutions. However, **P41** did not exhibit any signs of conjugation-length enhancement, and hence it appears that steric crowding in this material restricts the large degree of interaction with the LC solvent necessary to promote planarization. Consistently, only low

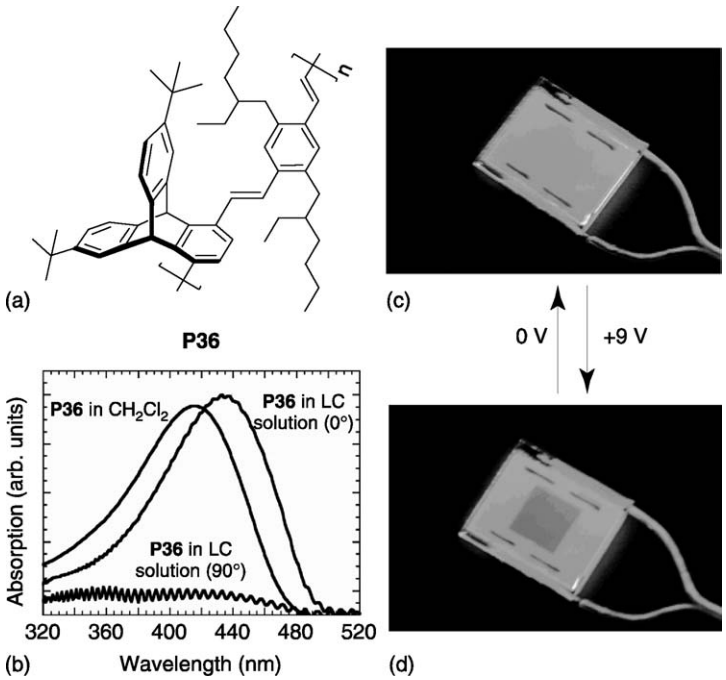

FIGURE 26 A nematic solution of PPV **P36** in **6CHBT**. The red-shift in the absorption spectrum of the liquid crystal solution is clearly apparent, and the alignment is apparent from the ratio of the spectra taken at 0° and 90° to the nematic director. The periodic signal at 90° is due to interference effects from the rubbed polyimide coatings of the test cell. The pictures document the fluorescence behavior of a **P36**/**6CHBT** nematic solution in a test cell. (c) A test cell is shown with no applied voltage, and the nematic director and polymer are aligned with the short axis of the cell. (d) 9 V is applied between the ITO pads on the top and bottom of the test cell that realigns the liquid crystal and polymer normal to the glass slides. This results in a dramatic reduction in the polymer's absorption and emission and complete loss of polarization.

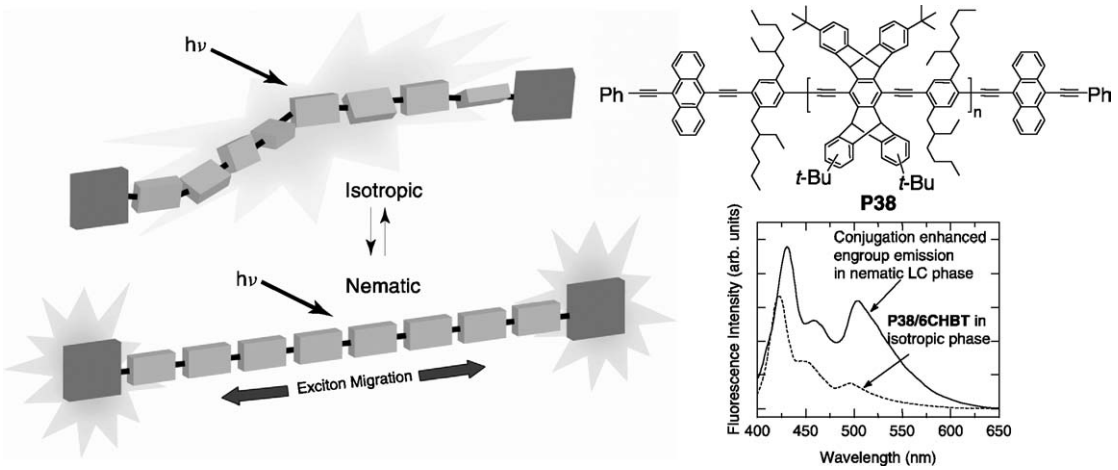

FIGURE 27 Conformational enhancement of energy transfer to low-energy trap sites located at polymer termini with nematic liquid crystals. Adapted with permission from ref. 33. Copyright 2005 American Chemical Society.

molecular weight versions of **P41** were soluble in the LC. In contrast, **P39**, with the least amount of steric congestion, showed the greatest amount of conjugation-length enhancement and the highest order parameter. Therefore, it is reasonable to conclude that the role of steric congestion about the polymer main chain plays an important role in determining the order parameter and conjugation-length enhancement in PPE–LC mixtures. Additionally, molecular weight dependent studies with **P39** revealed that order parameters as high as $S = 0.90$ can be achieved using samples with M_n greater than ca. 20,000.

Lastly, conformational and conjugation-length enhancements in PPEs are not only restricted to nematic LC solvents. Lyotropic LCs composed of water–potassium dodecanoate–decanol were also found to affect the same changes in PPEs

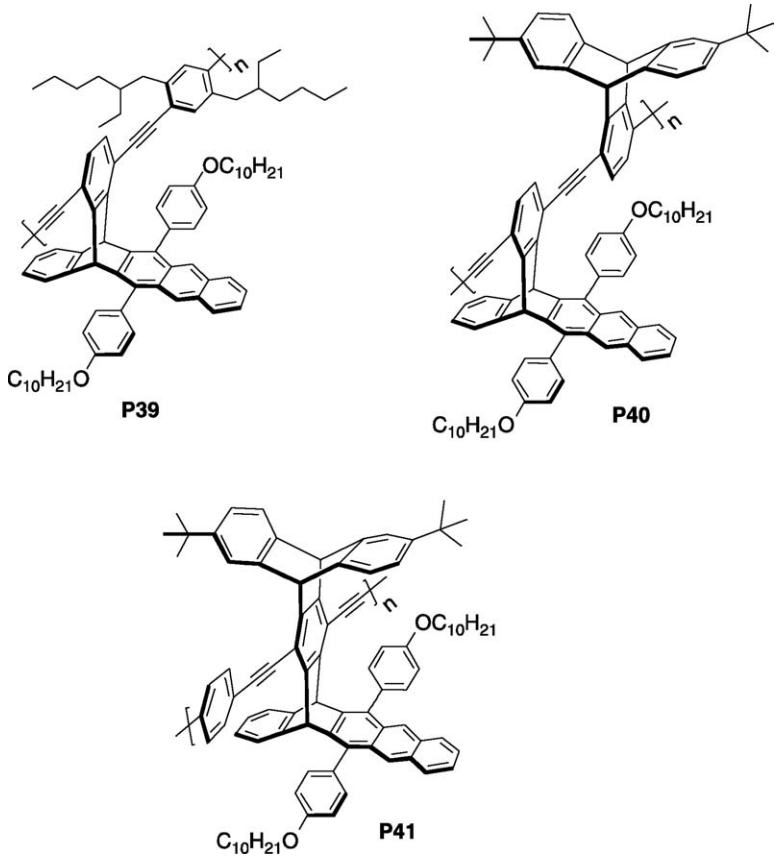

FIGURE 28 Structures of PPEs containing elaborate iptycene scaffolds.

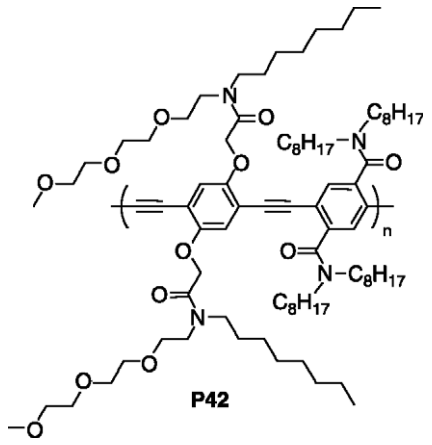

FIGURE 29 Structure of an amphiphilic PPE.

(e.g., **P42**, Fig. 29), provided the repeat unit of the polymer contained amphiphilic side chains.[35]

CONCLUSIONS

The ability of CPs to function as electronic materials is dependent on the efficient transport of excited states (excitons) along the polymer chain. Facile exciton migration in PPEs allows energy absorbed over large areas to be funneled into traps created by the binding of analytes, resulting in signal amplification in sensory devices. The energy migration in CPs can occur both *intra*molecularly and *inter*molecularly. In the case of dilute solutions, the *intra*molecular process dominates in the form of a 1D exciton random walk along isolated chains. Much higher efficiency can be reached in polymer aggregates and in solid films, where the energy migration occurs as a 3D process by both *intra*molecular and *inter*molecular pathways. The interplay between these two pathways has been a topic of contention, with intrachain migration being sometimes considered slow and inefficient as compared to its interchain counterpart. However, based on signal amplification of fluorescence quenching and efficient energy transfer to low-energy emissive traps in solution, we have shown that the intramolecular exciton migration in isolated polymer chains may indeed be very efficient.

A detailed understanding of intramolecular energy transfer in CPs can be elusive and is complicated by the conformational complexities that are typically associated with CPs in solutions and in thin films. LB monolayers constitute exceptions, as the rate of energy transfer can be investigated in PPEs assembled into discrete multilayers with precise control of polymer conformation and alignment. Kinetic analyses on LB multilayers surface modified with emissive traps indicated that energy transfer was much faster in the plane defined by each layer of the polymer chains as compared to the direction normal to the chains, thereby suggesting that *intra*molecular energy transfer is faster than the *inter*molecular process.

Fluorescence depolarization studies conducted on a family of triphenylene-incorporated PPEs with long lifetimes point to the through-bond Dexter energy transfer mechanism as being the dominant energy transfer pathway for *intra*molecular exciton diffusion. Extending the lifetime of a CP was universally found to increase the degree of *intra*molecular energy migration. Inclusion of structures with extended aromatic cores into the repeat unit of a PPE generally leads to an increase in the excited-state lifetime of PPEs. In addition, introduction of features that tend to localize excitations – such as biphenyl moieties, kinked polymer backbones, or exciplexes – into the polymer backbone also causes dramatic increases in excited-state lifetime. Generally, the photophysics of the chromophore monomer dictate the excited-state behavior of the corresponding CPs.

Emissive polymer films with modest to high quantum yields of fluorescence usually have limited electronic interaction between polymer chains, and in this case interchain energy migration is generally accepted to occur through the dipole-induced dipole mechanisms. The 3D nature of energy migration in films usually leads to longer exciton diffusion lengths, but often is accompanied by formation of low-emissive intermolecular species, resulting in diminished emission quantum yields. However, incorporation of rigid, 3D scaffolds, such as iptycenes and cyclophanes, can encourage an oblique packing of the chromophore units of a CP, thus allowing the formation of electronically coupled aggregates that retain high quantum yields of emission.

The rigid iptycene scaffolds also act as excellent structural directors that encourage complete solvation of PPEs in an LC solvent. LC–PPE mixtures display both an enhanced conformational alignment of polymer chains and extended effective conjugation lengths relative to isotropic solutions.

Note: a version of this Review appeared in the book "Charge and Exciton Transport through Molecular Wires", edited by Laurens D. A. Siebbeles, Ferdinand C. Grozema and published by John Wiley and Sons in January 2011 (ISBN: 978-3-527-32501-6).

REFERENCES AND NOTES

1 McQuade, D. T.; Pullen, A. E.; Swager, T. M. *Chem. Rev.* **2000,** *100*, 2537–2574.

2 McGehee, M. D.; Heeger, A. J. *Adv. Mater.* **2000,** *12*, 1655–1668.

3 Samuel, I. D. W.; Crystall, B.; Rumbles, G.; Burn, P. L.; Holmes, A. B.; Friend, R. H. *Chem. Phys. Lett.* **1993,** *213*, 472–478.

4 Goldfinger, M. B.; Swager, T. M. *J. Am. Chem. Soc.* **1994,** *116*, 7895–7896.

5 Schwartz, B. J. *Annu. Rev. Phys. Chem.* **2003,** *54*, 141–172.

6 Zhou, Q.; Swager, T. M. *J. Am. Chem. Soc.* **1995,** *117*, 7017–7018.

7 Allwood, B. L.; Spencer, N.; Shahriari-Zavareh, H.; Stoddart, J. F.; Williams, D. J. *J. Chem. Soc., Chem. Commun.* **1987,** 1064–1066.

8 Lakowicz, J. R. Principles of Fluorescence Spectroscopy; 3rd edn, Springer: New York, **2006**; pp 9–12.

9 Zhou, Q.; Swager, T. M. *J. Am. Chem. Soc.* **1995,** *117*, 12593–12602.

10 Swager, T. M.; Gil, C. J.; Wrighton, M. S. *J. Phys. Chem.* **1995,** *99*, 4886–4893.

11 Cotts, P. M.; Swager, T. M.; Zhou, Q. *Macromolecules* **1996,** *29*, 7323–7328.

12 Yang, J.-S.; Swager, T. M. *J. Am. Chem. Soc.* **1998,** *120*, 11864–11873.

13 Wegner, G. *Thin Solid Film* **1992,** *216*, 105–116.

14 Kim, J.; McQuade, D. T.; Rose, A.; Zhu, Z.; Swager, T. M. *J. Am. Chem. Soc.* **2001,** *123*, 11488–11489.

15 Satrijo, A.; Kooi, S. E.; Swager, T. M. *Macromolecules* **2007,** *40*, 8833–8841.

16 Satrijo, A.; Swager, T. M. *J. Am. Chem. Soc.* **2007,** *129*, 16020–16028.

17 Turro, N. J. Modern Molecular Photochemistry; University Science Books: California, **1991;** pp 357–359.

18 Yang, J.-S.; Swager, T. M. *J. Am. Chem. Soc.* **1998,** *120*, 5321–5322.

19 Sato, T.; Jiang, D.-L.; Aida, T. *J. Am. Chem. Soc.* **1999,** *121*, 10658–10659.

20 Bredas, J.-L.; Cornil, J.; Beljonne, D.; dos Santos, D. A.; Shuai, Z. *Acc. Chem. Res.* **1999,** *32*, 267–276.

21 Kasha, M. In Spectroscopy of the Excited State; Di Bartollo, B., Ed.; Plenum: New York, **1976**; pp 337–363.

22 Zahn, S.; Swager, T. M. *Angew. Chem. Int. Ed.* **2002,** *41*, 4226–4230.

23 Deans, R.; Kim, J.; Machacek, M. R.; Swager, T. M. *J. Am. Chem. Soc.* **2000,** *122*, 8565–8566.

24 Levitsky, I. A.; Kim, J.; Swager, T. M. *J. Am. Chem. Soc.* **1999,** *121*, 1466–1472.

25 Rose, A.; Tovar, J. D.; Yamaguchi, S.; Nesterov, E. E.; Zhu, Z.; Swager, T. M. *Philos. Trans. R. Soc. A* **2007,** *365*, 1589–1606.

26 Rose, A.; Lugmair, C. G.; Swager, T. M. *J. Am. Chem. Soc.* **2001,** *123*, 11298–11299.

27 Yamaguchi, S.; Swager, T. M. *J. Am. Chem. Soc.* **2001,** *123*, 12087–12088.

28 Tovar, J. D.; Rose, A.; Swager, T. M. *J. Am. Chem. Soc.* **2002,** *124*, 7762–7769.

29 Boden, N.; Movaghar, B. In Hand Book of Liquid Crystals: Low Molecular Weight Liquid Crystals; Demus, D.; Goodby, J.; Gray, G. W.; Spies, H. W.; Will, V., Eds.; Wiley-VCH: New York, **1998**; Vol. *2b*, Chapter IX, p 781.

30 Long, T. M.; Swager, T. M. *Adv. Mater.* **2001,** *13*, 601–604.

31 Long, T. M.; Swager, T. M. *J. Am. Chem. Soc.* **2002,** *124*, 3826–3827.

32 Zhu, Z.; Swager, T. M. *J. Am. Chem. Soc.* **2002,** *124*, 9670–9671.

33 Nesterov, E. E.; Zhu, Z.; Swager, T. M. *J. Am. Chem. Soc.* **2005,** *127*, 10083–10088.

34 Ohira, A.; Swager, T. M. *Macromolecules* **2007,** *40*, 19–25.

35 Bouffard, J.; Swager, T. M. *Chem. Commun.* **2008,** 5387–5389.